Die approbierte Originalversion dieser Diplom-/Masterarbeit ist in der Hauptbibliothek der Technischen Universität Wien aufgestellt und zugänglich.
http://www.ub.tuwien.ac.at

The approved original version of this diploma or master thesis is available at the main library of the Vienna University of Technology.
http://www.ub.tuwien.ac.at/eng

Unterschrift BetreuerIn

TECHNISCHE UNIVERSITÄT WIEN
Vienna University of Technology

DIPLOMARBEIT

Detecting Rubidium Atoms with a Nanofiber on a Chip

ausgeführt am Atominstitut
der Technischen Universität Wien

unter der Anleitung von
o.Univ. Prof. Dr. Jörg Schmiedmayer
assistiert durch Dr. Michael Trupke

durch

Anne Maître

Klimschgasse 28/18
1030 Wien

June 1, 2017

Unterschrift StudentIn

Abstract

This work describes several measurements made on a atom-cloud of ^{87}Rubidium with a tapered optical fiber. The atoms are loaded in a Magneto-Optical Trap, and detected with a Fabry-Perot cavity inside an optical nanofiber. The nanometer scale waist of the fiber leads to an evanescent light field, allowing the atomic photons to coupled into the fiber. Two Bragg gratings on both sides of the waist form a cavity for the atomic photons, enhancing their signal. The fiber is located just below an Atomchip, which leads to a great control over the cloud and the possibility of a one-dimensional trap matching the geometrical properties of the fiber.

In this thesis, the atoms are detected through the cavity, independently from the trap. Furthermore, methods for the confirmation of detection of a single atom at the fiber were analized. An optical dipole force was then implemented in an usual nanofiber to repel the atoms from the fiber surface, by building a barrier of potential with a blue detuned light.

Contents

1 Introduction **1**

2 Theoretical overview **4**
2.1 Laser cooling 4
2.2 Applications 8
2.2.1 Single atom detection 8
2.2.2 Bose-Einstein condensate 9

3 Experimental set-up **12**
3.1 Lasers set-up 13
3.1.1 External Cavity Diode Lasers 13
3.1.2 MOT 13
3.1.3 Lock 15
3.1.4 Control 16
3.2 Vacuum chamber 16
3.2.1 Dispenser 16
3.2.2 B-field configuration 17
3.3 Background considerations 20
3.3.1 Signal-to-noise ratio 20
3.3.2 Noise reduction 21
3.4 Control 21
3.5 Imaging system 23
3.5.1 Cameras 23
3.5.2 Measurements and pictures 24

4 Cavity **26**
4.1 Optical cavities 26
4.1.1 Basic properties 26
4.1.2 Atom-coupling cavity 28
4.2 Nano-fiber Bragg grating cavity 30
4.2.1 Tapered Optical Fibers 30
4.2.2 Implementation 31
4.2.3 Control 33
4.2.4 Utilisation 34

4.3 Rupture of the cavity 34
4.3.1 Finesse 35
4.3.2 Sticking atoms 36
4.3.3 Dust 37

5 Detection **38**
5.1 Absorption 38
5.1.1 Theory 38
5.1.2 Experimental implementation 39
5.1.3 Advantages and drawbacks 40
5.1.4 Typical measurements 42
5.2 Fluorescence 43
5.2.1 Theory 43
5.2.2 Experimental implementation 44
5.2.3 Advantages and drawbacks 45
5.2.4 Typical measurements 47

6 Photon antibunching **48**
6.1 Second order correlation function 48
6.2 Bunched, antibunched and coherent light 49
6.3 Detection 51
6.4 Background issues 56

7 Optical dipole force **59**
7.1 Atom-light interaction 59
7.2 Dipole force 60
7.3 Implementation 63
7.4 Results and discussion 65
7.5 Atoms and fiber surface interactions 69

8 Conclusion and outlook **71**

Bibliography **i**

1 Introduction

In the early twentieth century, a turning point took place in the scientific community with the very first steps of the quantum theory [1]. Many physicists stated revolutionary concepts, among them the wave-particle duality of light [2]. For centuries, scientifics had debated on this issue, wondering which of wave or particle description of light was the most adequate. The combination of both approaches was given with the quantum theory, which even went so far as to state that matter as well posseses wave properties (de Broglie's postulate). This was experimentally verified quickly afterwards, and was the starting point of quantum optics and a whole new understanding of matter.

While there were only few quantum experiments at that time, actual applications of this new effects came decades later, with the achievement of great new technologies like lasers, superconductors or semiconductors. More recently, lots of research were directed at cold atoms experiments, made possible through the development of atom optics in the late 80s [3, 4]. A new approach enabled scientists to reach much lower temperatures, reaching the microkelvin range. A whole new field of research was open, starting with the very first realisation of a Bose Einstein Condensate (BEC) in 1995 [5], 70 years after being predicted [6].

A BEC is a cloud of indistiguishable particles at very low temperature, which allows them to be all at the same quantum state of lower energy. Unlike matter-wave experiments with microscopic particles, a BEC has a macroscopic scale, which, among other things, enables to take actual pictures of a quantum system.

This research field quickly expanded in the following years : it reached multiple atomic species, investigated excitation spectra and effects of inter-particle interactions, leading to the realisation of molecular BECs and BEC-BCS crossovers. A wide range of research also focused on new effective way of trapping the atoms. Among other techniques, the atom chip technology has the benefit of an excellent control over the

atom cloud [7]. Forces from electric, magnetic and optical fields originate in microscopic structures built on the surface of the chip, and can manipulate motion and internal states of the atoms, confining them into micrometer sized region, at a temperature of a few hundred nanokelvins. Besides, the atoms are very well isolated from their environment, thereby having a decoherence time of tens of seconds.

In any case, most of our atomic knowledge comes from the study of atomic interactions with other entities, and in particular with light, easy to get and to detect. For strong interations, one needs a large electric field at the atom's position: a light beam confined to a small volume, typically of the atom-light scattering cross section size, suits well. This work is about an experiment which was designed to this end: a coherent light is confined in an optical fiber, tapered at a nanometer scale. This way, around the waist of the fiber, the light field is evanescent, as the fiber diameter is smaller than the light wavelenght: it can interact with the atoms present in this region.

In order to improve the detection, a Fabry-Perot cavity is built inside the fiber, using two Bragg gratings. Placed on both sides of the tapered region, they reflect every atomic photon around 20 times, increasing in the same time the electric field by the same factor. As they interact each time with the atoms, they increase the signal and help the filtering.

An important point to already keep in mind is that the cavity fiber is only used to detect the atoms: it plays absolutely no role in the trapping of them. They are trapped by external magnetic fields, and the center of mass motion is decoupled from the light within the cavity, resulting in a kind of hybrid quantum system.

The goal of this experiment is to build a good interface for atomchip: the combination of the two constituents, namely the nanofiber and the atomchip, provides the advantages of each of them. The chip enables traps with long coherence times and good control over the atoms, while the cavity fiber is a very efficient photodetector. The quasi one dimensionnality of both devices is one more argument for their combination.

This thesis is divided in two parts: an overall description of the experiment, followed by a report on the achieved measurements. First, after a theoretical overview, the experimental setup is outlined, with a focus

on the cavity properties and the detection methods. Afterwards, the photon antibunching of light and the optical dipole force measurements are presented.

2 Theoretical overview

In this chapter, a theoretical description of the experiment is made: in a first part the Magneto Optical Trap, or MOT, is explained. Different applications are then presented in order to get an idea of the possible goals and applications of such experiment.

2.1 Laser cooling

The MOT is achieved thanks to a technique of laser cooling. If the cooling effect of a laser can seem counter intuitive at first thought, it is actually very effective in some specific conditions.

Doppler cooling Considering a two-level atom with a lifetime τ and an atomic transition frequency ν_0, moving in the positive direction with a velocity v_x. The atom interacts with a counterpropagating monochromatic light wave of frequency ν_L (see figure 2.1) slightly detuned from the atomic transition: $\nu_L = \dfrac{c}{\lambda} = \nu_0 + \delta$.

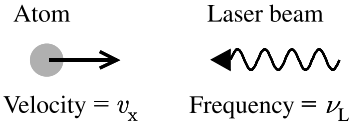

Figure 2.1: The frequency seen by an atom moving towards the laser is Doppler-shifted by $\nu_0(v_x/c)$ (Figure from [8])

The frequency of the laser seen by the atom is shifted by Doppler effect by an amount $\Delta\nu_L = -\overrightarrow{k}\overrightarrow{v} = kv_x$

Now, one photon of the laser beam can be absorbed by the atom, transferring to it its momentum $h/\lambda = \hbar k$. Whereas this momentum transfer is directed, as the laser field is unidirectionnal, the spontaneously reemitted photon is sent in a random direction, and have therefore an average momentum transfer of zero.

The ratio between the laser intensity I and the saturation intensity of the transition I_0 is the resonant saturation parameter $s = I/I_0 = 2\Omega^2/\Gamma^2$, where Ω is the Rabi frequency and $\Gamma = 1/\tau$ is the decay rate of the excited state. The average force on the atom is then [9]:

$$F_\pm = \pm\hbar k \frac{\Gamma}{2} \frac{I/I_0}{1 + I/I_0 + (2\frac{\delta \mp k v_x}{\Gamma})^2}$$

where the upper (lower) sign corresponds to a travelling plane wave propagating in the positive (negative) direction. This force, called radiation-pressure force, is in the direction of the propagation of the light. For high intensity ($I/I_0 \gg 1$), the maximal force is $\hbar k \frac{\Gamma}{2}$.

Optical molasses Now considering two counterpropagating beams, interacting independently with the atom. In the case of low intensities ($I \ll I_0$), the resulting force is the sum of each force $\vec{F}_+ + \vec{F}_-$:

$$\vec{F} = \vec{F}_+ + \vec{F}_- = \hbar\vec{k}\frac{\Gamma}{2}\frac{I}{I_0}\left(\frac{1}{1 + (2\frac{\delta - k v_x}{\Gamma})^2} + \frac{1}{1 + (2\frac{\delta + k v_x}{\Gamma})^2}\right)$$

For small velocities ($|kv| \ll \Gamma$ and $|kv| \ll \delta$), we obtain:

$$\vec{F} = 4\hbar\vec{k}\frac{I}{I_0}\frac{kv(2\delta/\Gamma)}{(1 + (2\delta/\Gamma)^2)^2}$$

For $\delta < 0$, this is a friction force, linear and opposing $\vec{v}$ (see figure 2.2). Because of the Doppler effect shifting the opposing laser beam closer to resonance, the atoms absorb more often photons from the counterpropagating beam than photons directing along their motion. The damping force can be written $\vec{F} = -\alpha\vec{v}$ with α the damping coefficient:

$$\alpha = -4\hbar k^2 \frac{I}{I_0}\frac{2\delta/\Gamma}{(1 + (2\delta/\Gamma)^2)^2}$$

When this one dimensional approach is extended to 3 dimensions, it is called optical molasses. An important point is that they only trap the atoms in a momentum space and not in a position space [9].

However, only the average light pressure was taken into account: this leads to a zero temperature state. This state is obviously non physical, as the isotropic radiation of the spontaneous emissions transfers a momentum $\hbar\vec{k}$ to the atom. Whereas the average velocity goes to zero, the average squared velocity does not, and counteracts the cooling effect. The Doppler cooling comes to a limit [10, 9]: for a laser detuning of $\delta = \Gamma/2$,

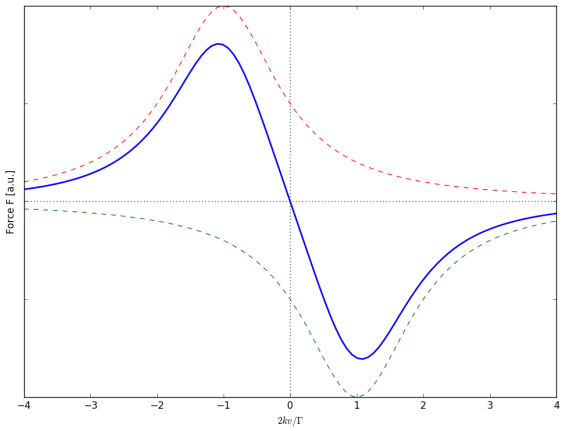

Figure 2.2: Total light force (blue line) versus velocity for $\delta = -\Gamma/2$ at low intensity. The dashed lines corresponds to the individual forces.

$$k_B T_{lim} = \frac{\hbar\Gamma}{2}$$

For ^{87}Rb the Doppler limit is $T_{lim} = 141\mu K$.

Magneto-optical trap For now, the atoms are only trapped in the momentum space: because of the thermal movement, the atoms diffuse. In order to get a proper trap in the position space, one needs to add a magnetic field and use the Zeeman effect [8].

Indeed, an external magnetic field produces an energy shift of the atomic states: the (2F+1) degenerate magnetic levels are split, with separations that increase linearly with the strengh of the field. In an inhomogeneous magnetic field $B(z) = az$, a two level atom with the ground state $|g, F = 0\rangle(m_f = 0)$ and the excited state $|e, F = 1\rangle(m_f = -1, 0, 1)$ have its excited state splitted into three Zeeman levels (figure 2.3). The resonance frequency of each component ($m_F = -1, 0, 1$) is different and depends on the position, except for z=0 where there is no splitting.

But the transition between the ground and excited states also depends on the polarization of the light. For an optical transition of $\Delta m_F = -1$, $\Delta m_F = 0$ or $\Delta m_F = +1$ respectively, a photon with a polarization σ^-, π or σ^+ respectively must be absorbed.

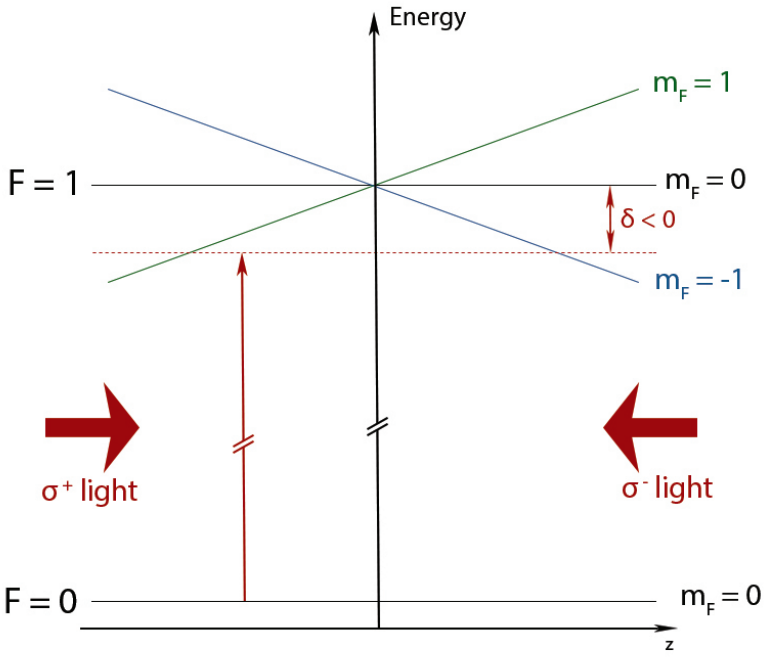

Figure 2.3: One dimensionnal MOT

In figure 2.3, a one dimensional MOT is represented, with two counterpropagating laser beams with opposite circular polarizations. In the $z > 0$ region, the energy of the $m_F = -1$ state is lowered, and therefore closer to the laser frequency. The right laser, σ^- polarized, is then able to excite the atom into this state $m_F = -1$. The resulting force, as explained earlier, pushes the atom back towards weaker magnetic field, i.e. towards the $z = 0$ point. Symmetrically, the σ^+ polarized beam adresses the atoms in the $z < 0$ region, where the $m_F = +1$ state is closer to resonance, pushing them back towards $z = 0$. This way, one gets a position dependent force, pushing the atoms towards one point: they are trapped.

Transfering this setup into three dimensions is quite simple: the easiest way is to use six counterpropagating beams with opposite circular polarization, and a B field distribution similar as $B(z) = az$, i.e. a quadrupole field (figure 2.4).

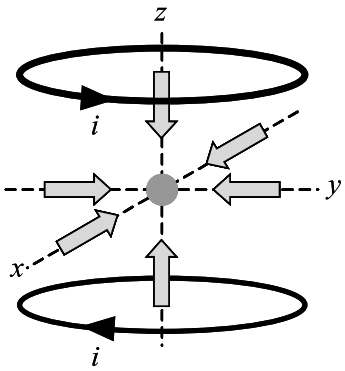

Figure 2.4: Geometry of a magneto optic trap [8]

2.2 Applications

The applications of this method are diverse, from ultracold Fermi Gases [11] to the cooling of a diatomic molecule [12]. However, this part will focus on two main applications, the single atom detection, which was already realised in a previous setup of this experiment, and the Bose-Einstein Condensation, which could be a next step of the current setup.

2.2.1 Single atom detection

Single atom detection is an important challenge in the developpement of atomic physics based quantum technologies, and the main problem lies in the way of performing such measurements with a robust and scalable technology.

Single atoms are very hard to detect, for the simple reason that they can only emit one photon at a time, and that as neutral particules, they do not interact strongly with the environnement.

The coupling of electromagnetic radiation and the atom is characterised by the scattering cross section σ_{scat}:

$$\sigma_{scat} = \frac{\sigma_{abs}}{1 + 4\Delta^2}$$

where σ_{abs} is the resonant scattering cross section and $\Delta = \frac{\omega - \omega_0}{\Gamma}$ the normalized detuning, with Δ the atomic line width.

The most efficient technique of detection is fluorescence [13, 14], i.e. the measurement of the scattered light. The signal must first of all be discriminated of the background light: indeed, only one nanowatt of background light generates around 4 billions photons per second, while an ^{87}Rb atom at its maximum emission rate would need 100 seconds to emit the same amount.

The presence of a cavity in the detection region is a very efficient way to enhance the atomic signal compared to the background light.

In a MOT setup, single atoms can obviously not be detected at the center of the trap. The challenge is to locate the MOT slightly away from the detection region, in order to consider only a peripheral part of it, where single atoms can be observed.

2.2.2 Bose-Einstein condensate

A Bose Einstein condensate (BEC) is macroscopical state of matter, composed of identical bosons, typically atoms, which, at a sufficiently low temperature, are all at the same unique quantum state of lower energy. Predicted in 1925 by Albert Einstein, who used the works of Satyendranath Bose, the first BEC was observed in 1995 by Eric Cornell and Carl Wieman, who received the Nobel prize in 2001.

Ultralow temperature physics made huge improvements with the developpement of laser cooling [15]. It allowed the use of room-temperature vacuum chamber, with very easy optical access compared to old cryogenic cells with multi-layers schielding. It also increased the number of atomic species to be studied, from helium and hydrogen to all of the alkali atoms, metastable rare gases and several earth alkali atoms [16, 3, 17].

To create a BEC in a dilute gas, one needs to cool down and compress the atoms in a trap, until the de Broglie wavelenght is in the order af the interatomic space [15]. This is done in high vacuum chamber by using magnetic trap or laser light: those traps can store atoms for enough time (seconds or minutes) for them to be cooled down in two steps.

Indeed, conservative atom traps can only confine neutral atoms with an energy lower than 1 Kelvin: a pre-cooling is therefore necessary. The atoms are then compressed in a magnetic trap in order to get high collision rate and effective evaporative cooling [15].

In most of BEC experiments, pre-cooling is realised with a Magneto-Optical Trap. The temperature is then limited by heating due to spontaneaous emission, and density by radiation trapping effects and trap loss due to excited-state collisions. It leads to $T \sim 50\mu K$ and a density of $\sim 10^{11}$ cm^{-3}, while after the evaporative cooling, the atoms will be at 500 nK and 10^{14} cm^{-3} [15].

Conservative atom traps keep the atoms compressed during cooling, and later hold the condensate for study. Several traps with small enough heating rate are possible, realised with ac or dc magnetic fields, or far-off-resonance laser beams [15]. The most common ones are Ioffe Pritchard traps or Time-averaged Orbiting Potential traps (TOP).

Magnetic traps only confine weak field seeking states, which means that atoms making a transition into a strong field seeking state are lost from the trap. The trap is only stable if the atom's magnetic moment adiabatically follows the direction of the magnetic field, i.e. if the rate of change in the field's direction θ is slower than the magnetic moment [15]:

$$\omega_T = \frac{d\theta}{dt} < \frac{\mu_m |B|}{\hbar} = \omega_{Larmor}$$

ω_T is the trapping frequency.

The Ioffe Pritchard trap [18] is an harmonic trap producing a tight trapping potential. It is the tighest trap which can have a bias field: the axial field is therefore $B_z = B_0 + B''z^2/2$, while the leading term of the transverse field component is linear: $B_x = B'x$. After full compression to a final temperature T, the equivalent radial curvature is $\mu_m B'^2/k_B T$.

A TOP trap is a linear trap, with a rotative magnetic bias field to compensate the trap losses due to Majorana flips in addition to a spherical quadrupole field. The frequency of the rotating field must be higher than the orbiting frequency of the atoms, but lower than the Larmor frequency, typically $\omega_{Larmor} \approx 7$ MHz [19].

The angular frequency of the atoms in a quadrupole trap is given by [4]:

$$\omega_{at} = \sqrt{\frac{a}{\rho}} = \sqrt{\frac{\mu_B \nabla B}{M\rho}}$$

with a the centripetal acceleration, μ_B the Bohr magneton, M the atomic mass and ρ the radius of the atomic circular orbit, i.e. the size of the trap.

In our experiment, in order to create a BEC, the most appropriate trap would be a TOP trap. In this case, the trap frequency ω_T would need to verify $\omega_{at} < \omega_T < \omega_{Larmor} \approx 7$ MHz

And concerning ω_{at}:
$\mu_B = 9.27 \cdot 10^{-24}$ J/T
$M(^{87}Rb) = 87 \cdot 1.66 \cdot 10^{-27}$ kg
$\nabla B \approx 120$ G/cm= 1.2 T/m

which means, for a MOT of 3 mm:

$$\omega_T \approx 160 \text{ Hz}$$

The eventual trap frequency would need to be between:

$$160 \text{ Hz} < \omega_T < 7 \text{ MHz}$$

3 Experimental set-up

The goal of this experiment is to create a Magneto-Optic Trap (MOT) for the D_2 transition of ^{87}Rubidium atoms, and to detect them using nanofibers. First, the lasers beams need to be created, shaped and controled, before being send into the vacuum chamber. Within, there is a background Rubidium gas, and a magnetic quadrupole trap, so that a MOT can be loaded and detected. An usual external imaging system can be used, or measurements can be done with one of the two nanofibers present in the chamber: a regular optical nanofiber, or a Bragg grating nanofiber cavity (see chapter 4). A schematic overview of the set-up is given in figure 3.1.

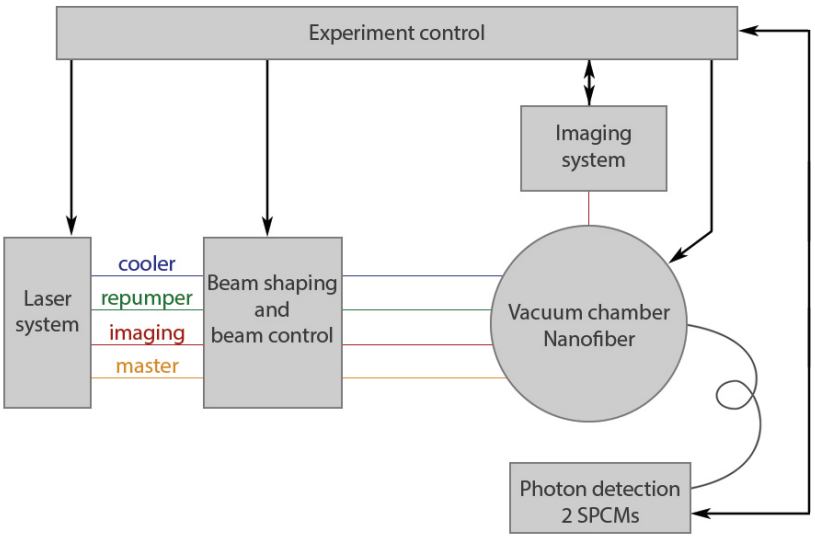

Figure 3.1: Structural overview of the set-up

3.1 Lasers set-up

The Doppler cooling of the MOT obviously uses lasers. If in theory only one cooling laser should be enough, the actual set-up is in reality more complicated, and is presented in this section.

3.1.1 External Cavity Diode Lasers

In atomic physics, diode lasers are commonly used due to their low cost, flexibility and ease of operation [20]. If the resonator lenght of a laser diode is typically around 300 μm, which is usually quite small, it is not enough to make a MOT. Thus External Cavity Diode Lasers (ECDL) are used in such experiments, as the increase of the cavity length stabilises the frequency. This way, the linewidth can be reduced to below 1 MHz.

ECDL lasers can be used in two different configurations: Littrow's [21] or Littman's [22]. The Littman configuration allows more frequency stability and a wider range, whereas in the Littrow configuration more power can be send. As the frequency changes during operation are quite small (around 10 MHz), small beam displacements can be more easily tolerated than some drops in power [14]: all our lasers are in the Littrow configuration.

3.1.2 MOT

In our experiment, four lasers are in use: the cooler and the repumper, essential to the MOT generation, the imaging laser for the different measurements, and the master laser, used as a locking reference and which could also be used as an optical pump. They all have different positions in the hyperfine structure of the ^{87}Rb D_2 transition, as represented in figure 3.2.

The cooling laser handles the cooling cycle, being slightly red detuned ($\Delta \sim$10 MHz) from the $F = 2 \rightarrow F' = 3$ transition. It also needs the highest power in order to trap the maximum number of atoms: after being amplified by a tapered amplifier, and going through a AOM driver as a control system, around 400 mW are sent in the chamber.

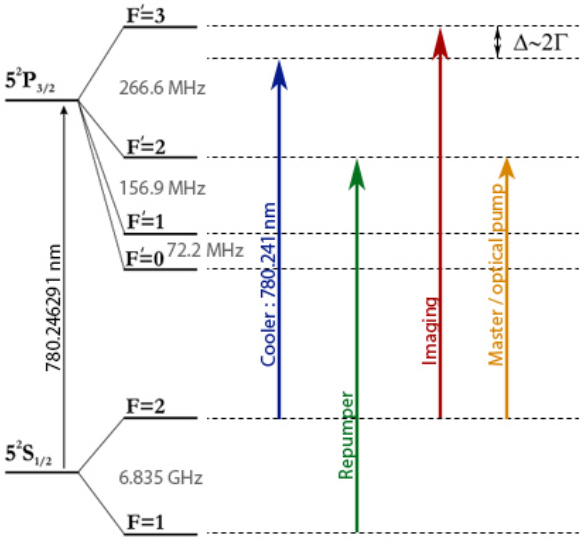

Figure 3.2: ^{87}Rb D_2 transition hyperfine structure and all the lasers used in the experiment

However, once every thousand cooling cycles, the atom does not decay into the F=2 state: it falls up to the F=1 state or dark state, and leaves the cooling cycle. The repumper laser can then reexcite it into the F'=2 state, from where it will decay in the F=2 state and join again the cycle.

With these two lasers, the MOT is complete: it now needs to be detected. The imaging laser will allow it, either with time of flight pictures, or using absorption or fluorescence detection (see Chapter 5). As it needs strong coupling to the atoms, it operates on the $F = 2 \rightarrow F' = 3$ transition.

Finally, an optical pump can also be used in order to realise a proper magnetic trap. It will stock all the atoms in the $5^2S_{1/2}|F = 2, m_F = 2\rangle$ ground state, contrary to a MOT where all magnetic sublevels are traped. It provides this way less losses and therefore a better cooling and a denser trap. However, as it was not necessary for our measurements, it was not in use.

The lasers have different powers: in order to get a consistent MOT, it is important to have enough cooling power. In this case, after going through a tapered amplifier and some AOM, around 300 mW of cooling

light were send into the chamber. For the other lasers the power question is less important: for the imaging for example, it makes no sense sending higher power when the atoms already saturate. It could actually be a problem in absorption since the SPCM become non-linear for too high amount of counts.

Concerning the beams, the cooler is not split up in six counterpropagating beams as usual, but only in four: two horizontal ones, and two diagonal ones, which reflect on the chip as a mirror (see figure 3.3). This way, one incident beam and its refleted one are seen by the atoms as two counterpropagating beams. So there is a Doppler cooling in the central zone where all the beams superimposed, as the atoms feel six counterpropagating beams from the three different directions. This kind of MOT is commonly used and is called a mirror magneto-optic trap (MMOT) ; further details can be found in [23] or in [24].

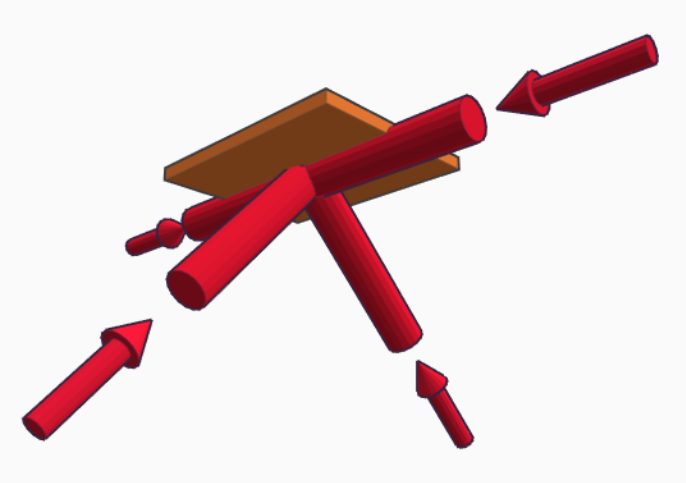

Figure 3.3: Cooler beams geometry in a mirror MOT

3.1.3 Lock

In order to stay at the exact desired frequency, the lasers are locked, using a frequency modulation (FM) locking technique relative to an atomic transition or a frequency offset (FO) locking technique relative to a reference laser, called master. This is why the optical pumping laser is actually used only as a master laser, to which the imaging and the cooler are locked. As for the repumper, more than 6 GHz away, it is locked on

its own with a FM technique. All the locks are explained in detail in Marco Wilzbach's master's thesis [25].

3.1.4 Control

The lasers beams are controlled using Acousto-Optic Modulators (AOM). Those devices use the acousto-optic effect to defract the light frequency [26]. They are powered in RF by AOM drivers, which are controlled via an analog input directly connected to the Adwin control system. The AOMs can precisely shift the detuning of the light, as well as switch the beams on and off. In most of cold atoms experiments, mechanical shutters are used: indeed, the AOMs always let some leak through. However, it is not the case here: a mechanical shutter leads to mechanical noise which our nanofiber will perceive, and which will be seen in the measurement as a huge noise. This is why the mechanical shutters are not used in every cycle but stay open during the measurements.

The locks are very sensitive to the vibrations of the laser cavity: in order to increase stability and to keep the different parts of the experiment independent, the laser beams are fiber coupled. As they all need to be controled by an AOM and cross a mechanical shutter, those have been integrated to the laser setup before fiber coupling, when possible. The main exception remains for the cooler, which needs a Tapered Amplifier (TA): its efficiency and stability depends greatly on the short path to the fiber coupler, which is why the AOM and the shutter were placed after the fiber.

3.2 Vacuum chamber

In order to optically cool down the atoms, they must be isolated from the environnement and in a sufficiently low vaccum. A vaccum chamber is therefore used, with several windows to ensure the different light beams to enter.

3.2.1 Dispenser

The MOT setup traps the atoms of the rubidium gas present in the chamber. It comes from a ^{87}Rb dispenser: it is mainly a reservoir of solid Rubidium embedded in a wire. By running some current through, it will heat up the Rubidium and lead to its evaporation.

It is important to notice that this is a thermal phenomenon: the turning on or off of the dispenser changes the temperature in the chamber, and a new equilibrium must be found before starting any new measurements. The most evident example is the locking of the cavity: by turning on the dispenser after a week-end off, one must wait for around 10 minutes before being able to lock the cavity.

The intensity of the current running through the dispenser is also significant: it will change the temperature and the density of Rubidium atoms in the chamber. It is therefore not possible to compare measurements if the dispenser current for each of them is not the same.

3.2.2 B-field configuration

B-field generation In addition to the laser cooling of the atoms, a MOT requires a quadrupole magnetic field. Ours is a superposition of a cylindrical magnetic field created by a wire and two homogeneous orthogonal magnetic fields created by coils outside the chamber. The issue with this configuration is that the structures are quite large, so the field gradient is limited.

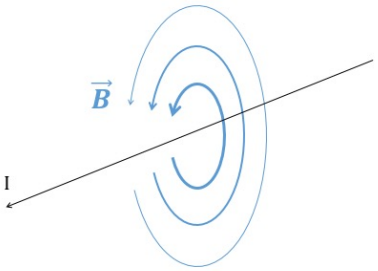

Figure 3.4: Geometry of the magnetic field created by a single wire

The main idea is simple: the magnetic field generated by a wire (see figure 3.4) has a cylindrical geometry. It must be compensated in one point in order to be able to create a MOT. To do so, two homogeneous fields are applied using coil pairs, orthogonal to the wire axis (see figure 3.5)

Copper structure The cylindrical field is actually not generated by a usual wire: a copper structure is placed on top of the chip, with an elec-

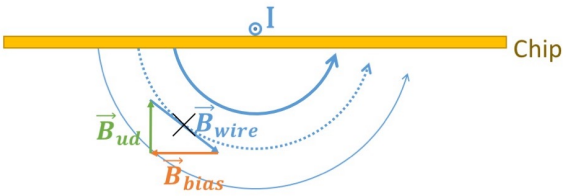

Figure 3.5: B field configuration in a plan orthogonal to the current: in blue, the magnetic field generated by the wire ; in orange and green, the two components of the homogeneous magnetic field created by the coil pairs, compensating the cylindrical field in one point

trical current running through it (see figure 3.6). The copper structure has a H form, in order to be used either in a U or in a Z configuration, even if in our case, it was only in a U configuration.

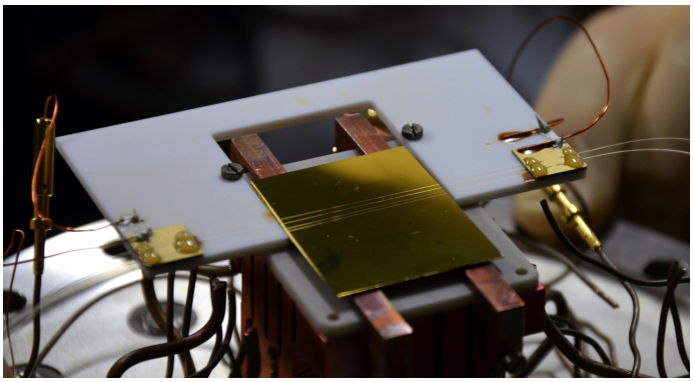

Figure 3.6: Mount picture

But a "U" can be form in two ways: in figure 3.7, all the devices next to the chip are represented. The piezos were initially designed to be able to control three fibers. However, the pulling operation is a meticulous process, as well as the construction of a Bragg grating cavity on an optical fiber. Out of the ten cavity fibers initially produced, only three had sufficient properties. Out of this three cavities, only one survived the pulling process. This is why only one cavity fiber was put into the chamber, along with an usual nano-fiber, which could be useful for some preliminary measurements, but is a very less sensitive detector than the cavity, and it was not worth putting two of them in the chamber.

So from the three places for fibers on the piezos, only two are occupied: the center one is occupied by the usual fiber, and the right one (see figure 3.7) by the cavity one, which means that the cavity is off center from the H bar. So the configuration of the current in the copper is not insignificant: the gradient of the magnetic field will be different. In figure 3.7, the magnetic field gradient from the green current I_1 is lower at the cavity position than the gradient from the red current I_2.

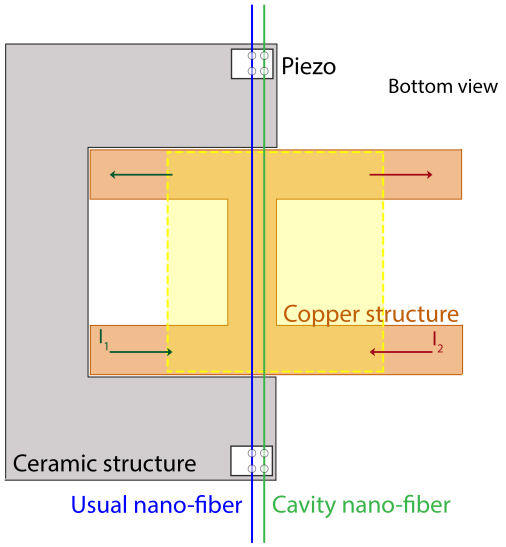

Figure 3.7: Copper structure from bottom view. In yellow, the position of the chip, placed in between the copper structure and the fibers. The green current I_1 corresponds to the initial configuration, the red one I_2 to the configuration after the change of the cooling laser, in order to have a higher gradient at the fibers.

A higher gradient means a smaller but denser MOT, which is better for our purposes. But when the experiment was first setted up, the I_1 current was configurated. It stayed this way for some time, until the diode of the cooler laser broke and needed to be changed. As a lot of parameters needed to be recalibrated in order to get the MOT back, it was the opportunity to also change the copper configuration into the I_2 current.

3.3 Background considerations

In cold atoms experiments, the background noise can be strong compared to the signal. It is therefore important to reduce it as much as possible in order to get processible data.

3.3.1 Signal-to-noise ratio

The noise in the photon detectors data mainly comes from the background light, but also from some detectors defects.

The photon detectors used in the experiment are two Single Photon Counting Modules (SPCMs). Those modules are actually composed by an SPAD (single-photon avalanche diode) with active quenching circuit, internal bias voltage generation and stabilization, thermal stabilization, and electrical and optical connectors. Their operation is explained more detailled in [14].

The main noise from the detector defects are the dark counts, avalanches ignited by thermally activated electrons. Acording to the manufacturer (Perkin Elmer), they are supposed to be lower than 500 counts/s, which corresponds to the measured values of 245 ± 10 cps (counts-per-second) and 304 ± 12 cps.

The background light has different sources, as listed in table 3.1

Background light sources	
TSP	$\gg 15.10^6$ cps
MOT beams	$\gg 15.10^6$ cps
vacuum gauge	$0, 24.10^6$ cps
ambient light	4800 cps
^{87}Rb dipsensers	3000 cps
probe beam	30 cps/nW

Table 3.1: Background contributions, if left unshielded, listed by source [14]

Ambient light is a major source but can be easily well reduced, whereas sources inside the chamber are more tidious to shield. Those are from two kind: black body radiation, from the hot vacuum gauge, the ^{87}Rb dispensers and the titan sublimation pump (TSP, always off when measuring) ; and scattered light from the laser beams (mostly the cooler ones) which couples into the fiber and leads to background counts.

The background light can also be deleted afterwards. For that, one introduces the signal-to-noise ratio:

$$SNR = \frac{S}{N}$$

where S is the signal power and N the noise power.

3.3.2 Noise reduction

Most of the major background sources can be easily shielded or completely turned off. This is the case for the titan sublimation pump, which is always turned off when measuring, or for the MOT beams, which are usually switched off using AOMs during each measurements.

However, as explained earlier, no mechanical shutters are used during measurement: that is why the earlier beams can also induce scattered light which can be perceived by our very sensitive detectors. In order to remedy this, several stages of cloth and metal separation walls are introduced between the laser shutters and the vacuum chamber, reducing stray light in the detector to non-measurable values.

The vacuum gauge can as well simply be turned off. Ambient light is suppressed by surrounding the optical table from all six sides by optically dense materials.

If this is not enough, a filter can be use: an optical bandpass filter with 99.5899% transmission at 780 nm and 3 nm bandwidth (FWHM) [27]. Using this filter can reduce ambient ligth from 4800 cps to 0 cps, as well as the dispenser light from 3000 cps to 36 cps. Therefore, it allows continuous operation of the dispensers and normal lab operation including monitors and room light without influence on the measurements. To this 36 cps bust be added the contribution of the probe beam, 30 cps, which leads the background light contribution to around 66 cps.

Total background rate The typical total background rate bg for a single counter is the sum of the dark counts and the above background light contribution, i.e. $bg = (245 + 66)$ cps $= 311$ cps.

3.4 Control

The control of this experiment is accomplished by a Matlab program called Adwin. It controls two kind of channel, analog or digital. Among

the analog ones, one can find for example the three components of the magnetic fields, or else the intensity or detuning of the lasers (see figure 3.8). For the digital ones (laser TTL trigger, counter gate...), only the first state (high or low, i.e. beginning with 1 or 0) and the delay between each switch is necessary.

Figure 3.8: Adwin window for the analog channels: in each case is precised the initial value (upper right), the shape (ramp or constant, upper left) and the time to consider (down)

One important part of the setup is the timing coordination. All timings are indicated in milisecond, and the devices are quick enough to follow the signal in the same time scale.

The variables are also of two kind: independent ones, which can be manually changed in the variables window, and some which depend on others, which formulae are entered as calculated variables.

The program was first designed for a BEC experiment, so for cycle around 30 s. In our case, a MOT needs to be load for only a couple of seconds (usually 3 s). But at the end of each adwin cycle, the program needs a couple of second to process. In order to avoid to have this delay every time, we usually use some subcycles inside the adwin cycle, and the restricted factor actually became the number of cases per cycle in the program.

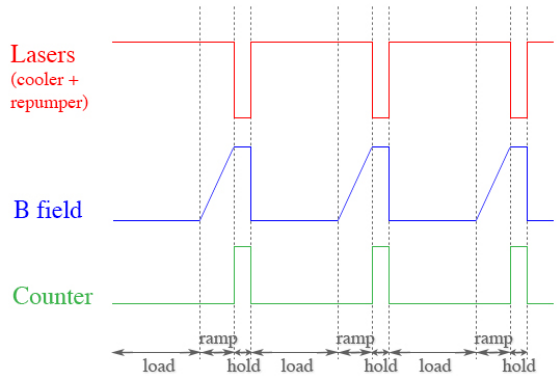

Figure 3.9: Example of the timings for one cycle with 3 subcycles

Figure 3.9 shows the behavior of different parts of the experiment for a usual cycle including three subcycles. As the MOT is usually loaded away from the chip, and therefore from the fibers, it needs to be magnetically led toward the fibers, hence the ramp in the B field. The cooler and repumper are obviously essential for the MOT, but are a huge source of noise during the measurements: they are switched off when the counter turns on.

3.5 Imaging system

A last part of the set-up consists in the imaging system: it is used not only to see what is going on in the chamber, but also to make basic measurements such as the atom number, which can be determined with a single shot picture.

The imaging system is well decribed in Michaela Wagner's masterthesis [28], which is why only an overview will be given here.

3.5.1 Cameras

A first very basic camera is constantly on in order to see the outside of the chamber, and be aware of the main settings, like if the lasers are on or off or if the MOT is there.

Two PixelFly cameras are also in used in the experiment: one on the side, orthogonally to the fibers, and one on the bottom, to see the chip and the fibers from below. They are both Pixelfly-QE from the company PCO, digital 12 bit CCD cameras, and have a quantum efficiency of around 30% for a 780 nm laser. They have 1392 x 1024 pixels and an imaging region of 5.2 x 3.8 mm.

The camera on the side is particularly used for pictures of the MOT in time-of-flight: this gives some immediate data on the cloud, like the atom number, or also its size and its density.

Finally, a last camera is also placed on the side of the chamber: an Andor Ikon-M camera from Andor Technology. It is a back illuminated deep depletion CCD camera, with 1024 x 1024 pixels and an imaging region of 2.4 x 1.2 mm, so a smaller field of view than the Pixelfly (see figure 3.10). However, at 780 nm, the quantum efficiency is above 90%, which means that nearly every incoming photon gets detected.

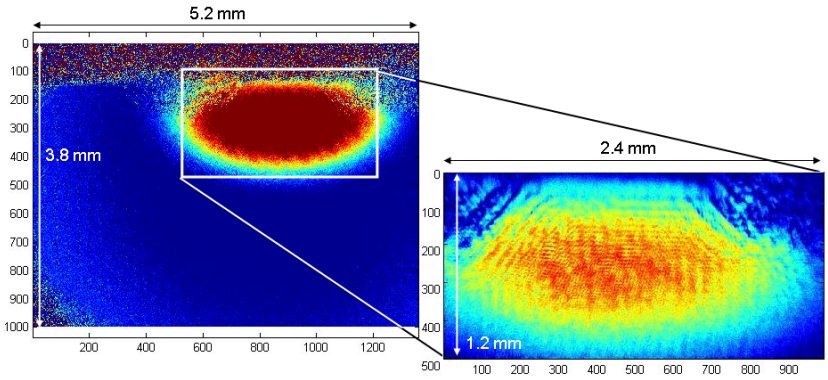

Figure 3.10: Comparison of the imaging regions: Pixelfly left, Andor right [28]

3.5.2 Measurements and pictures

The measurements in time of flight (TOF) use the absorption principle: two pictures are taken at 20 ms intervall, with and without atoms, and are substracted. The imaging beam comes from outside of the chamber, orthogonaly to the fibers. It goes trough the MOT and get collected by the camera (see figure 3.11).

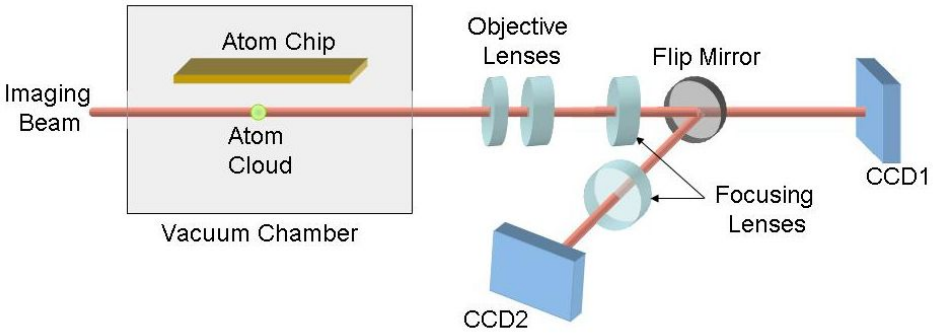

Figure 3.11: Imaging system configuration [28]

The first picture (see figure 3.12a) is taken imediatelly after the shut off of the MOT lasers, so that the atom cloud is still there. As the acquisition time of the camera can be quite long, the imaging light only flashes for 0.1 ms and everything else is off for the rest of the aquisition. 20 ms later, the second picture (figure 3.12b) is taken, in exactly the same conditions as the first one, except that the atom cloud has expended and fallen and is no more in the picture. The substraction of the two pictures gives the image of the MOT, and some fit program calculate its size, atom number and other properties.

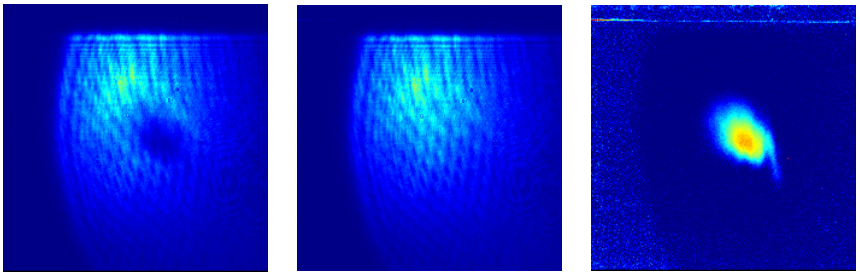

(a) With atoms (b) Without atoms (c) Absorption image

Figure 3.12: Absorption pictures: left, the first picture taken with the atoms ; center, the second one without the atoms, and right, the absorption picture is the difference of the two first ones.

4 Cavity

The main specificity of the experiment is the use of a Fabry-Perot cavity inside one of the nanofiber, completely independent of the atomic trap. It is detailled in this section, after a reminder of the cavity theory.

4.1 Optical cavities

4.1.1 Basic properties

The basic properties can be illustrated in the simplest case of optical cavities, namely a planar cavity. A planar cavity (see figure 4.1) consists of two plane mirrors M_1 and M_2, respectively with reflectivity R_1 and R_2, separated by an adjustable length L_{cav}. The cavity is filled by a medium of refractive index n. It basically works as a Fabry Perrot interferometer for light of wavelenght λ, as the two mirrors are parallel aligned.

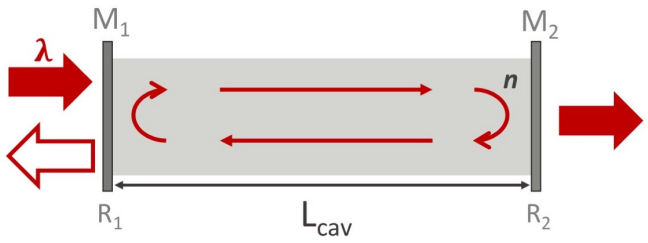

Figure 4.1: Planar cavity

The first main property of a cavity is the transmission T: how much of the input power get through. It is simply given by:

$$T = \frac{T_n}{T_c}$$

where T_n is the output power and T_c the input power, so it is easily measurable.

Under the assumption of no absorption nor scattering loss within the cavity, the transimission is also given by [8]:

$$T = \frac{1}{1 + (\frac{2F}{\pi})^2 sin^2(\frac{\phi_{rt}}{2})}$$

where:

- $F = \dfrac{\pi(R_1 R_2)^{1/4}}{1 - \sqrt{R_1 R_2}}$ is the finesse of the cavity
- $\phi_{rt} = \dfrac{4\pi n L_{cav}}{\lambda}$ is the round trip phase shift

The cavity is on resonnance when the transmission is equal to 1, i.e. when $\phi_{rt} = 2\pi m$, which amounts to

$$L_{cav} = \frac{m\lambda}{2n}$$

An other useful parameter is the full width at half-maximum (FWHM). Given that the transmission is a sharply peaked function of the round trip phase shift, the width of the peak can be easily calculated using a transmission $T = 50\%$. In the limit of a large finesse, we obtain $\phi_{rt} = 2\pi m \pm \pi/F$, which then leads to:

$$\Delta\phi_{FWHM} = \frac{2\pi}{m}$$

and a new definition of the finesse:

$$F = \frac{2\pi}{\Delta\phi_{FWHM}}$$

The finesse of the cavity can thus be described as the ratio of the separation between adjacent maxima to the half width.

The finesse of a cavity is linked to the number of round trip of the photons. In our case, the photons are refleted circa 20 times before leaving the cavity, leading to a finesse $F \approx 65$. It is way below the best existing cavities, but quite standard for a Bragg-grating one.

A resonant cavity leads to resonant modes: all modes of the light that satisfied the resonance condition are preferably selected by the cavity, and have larger amplitudes. All waves are in phase and therefore lead to constructive interferences.

The frequencies of the resonant modes are given by:

$$\omega_m = m\frac{\pi c}{nL_{cav}}$$

and using the proportionnal relation between mode frequency and phase, as well as the definition of the full width at half-maximum, we obtain:

$$\Delta\omega = \frac{\pi c}{nFL_{cav}}$$

It is also usefull to know the photon lifetime τ_{cav} inside the cavity. We consider a symmetric high finesse cavity with $R_1 = R_2 = R \approx 1$, at the center of which a light source emits a short pulse of light into the cavity mode, containing N photons. Each time the pulse meets one of the mirrors, $(1 - R)N$ photons are lost, i.e. every $\Delta t = nL_{cav}/c$. This allows us to introduce the photon lifetime in the cavity τ_{cav}:

$$\tau_{cav} = \frac{nL_{cav}}{c(1 - R)}$$

as well as the photon decay rate κ:

$$\kappa = \frac{1}{\tau_{cav}}$$

It is important to notice that under the previous conditions, $\Delta\omega = \tau_{cav}^{-1} = \kappa$. This shows that the width of the resonant modes is controlled by the photon loss rate in the cavity, in exactly the same way that the natural width of an atomic emission line is controlled by the spontaneous emission rate [8].

Finally, only two parameters are necessary to describe the cavity: the resonant mode freqeuncy ω_m and the finesse F, all others being related to those two.

4.1.2 Atom-coupling cavity

The interactions between light inside a cavity and a two level atom are also relevant in our case. In the following section will be presented a few usefull parameters to best describe what happens in the cavity.

The interesting case is when the transition frequency of the atom correponds to one of the resonant modes of the cavity, so that atom and cavity can exchange photons in a resonant way. We also consider that the transition frequency of the atom is fixed (it is true for atoms in vacuum, however, we will see that it can be shifted due to some interactions. In particular, it is completely different when the atoms stick to the fiber surface and can no longer be considered as atoms in vacuum.).

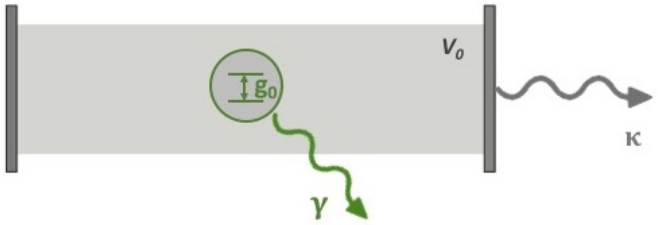

Figure 4.2: A two level atom in a resonant cavity with modal volume V_0

At resonance, as represented in figure 4.2, the relative strenght of the coupling is described by three parameters:

- the photon decay rate of the cavity κ, as defined in the previous section
- the non-resonant decay rate γ, depending on the atom and the considered transition
- the atom-photon coupling parameter g_0, which describes the atom-cavity coupling

From those parameters, the atom-cavity coupling can be defined as a **strong coupling** when $g_0 \gg max(\kappa, \gamma)$, and as a **weak coupling** when $g_0 \ll min(\kappa, \gamma)$.

A strong coupling corresponds to a reversible emission of a photon: a photon emitted by the atom is re-absorbed by it before leaving the cavity. Conversely, in a weak coupling, the emission of a photon is irreversible, even if the cavity affects the emission rate.

In order to study the atom-cavity coupling, one needs to know the relative magnitudes of κ, γ and g_0.

In the case of our cavity, those parameters are:

- $\kappa \approx 2\pi \cdot 9.1$ MHz
- $\gamma \approx 2\pi \cdot 3$ MHz
- $g_0^{max} \approx 2\pi \cdot 1.3$ MHz the maximum single atom coupling rate
- $g_{eff}^{max} \approx 2\pi \cdot 38.5$ MHz the maximum collective atom coupling rate

Those values of the atom coupling rates are *maximum*, because they actually depend on the time considered. Indeed, the coupling of the atoms in the cavity changes in time: it is strong at the beginning of the measurement, just after the shutting off the MOT lasers, when the cloud is still dense and cold ; then it progressively decays to a weak coupling with the heating and expansion of the cloud.

4.2 Nano-fiber Bragg grating cavity

In this experiment, the optical cavity is actually a Bragg grating cavity in an ultrathin optical fiber. It combines the properties of a usual optical cavity, as described earlier, and of a vacuum-clad subwavelenght-diameter optical fiber, as will be discussed.

4.2.1 Tapered Optical Fibers

Tapered Optical Fibers are commercial single mode optical fibers which have been pulled until having a nanometer scale waist. Every guided light through the fiber generates an evanescent light field around the fiber in the waist region, and have a strong radial confinement of the light [29]. It offers several possibilities of interations between light and matter, for examples by coupling particles (atoms, molecules, quantum dots... [30]) on or near the fiber surface to the guided fiber modes. For example, absorbance of organic dye molecules deposited on a tapered fiber can be measured with high sensitivity, fluorescence of a small number of irradiated atoms have been spectraly analyzed, or atomic traps around the fiber using the optical dipole force from the evanescent field have been build [30].

Tapered optical fibers only have a waist of a few centimeters. In order to keep a good transmission, the radius evolution must not be too abrupt (see figure 4.3). For technical reason, it is also better to keep the waist rather small [29].

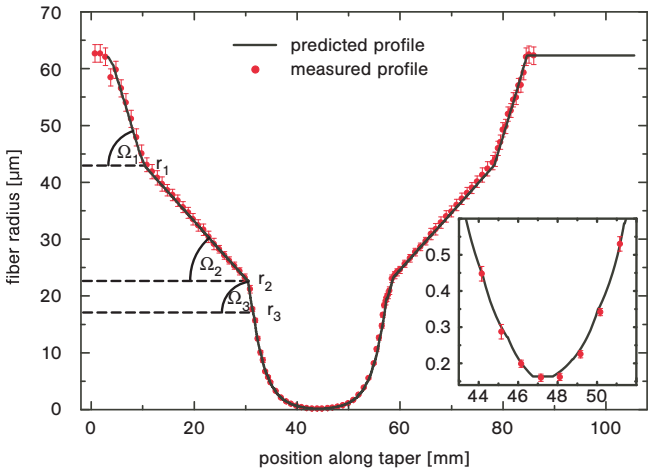

Figure 4.3: Typical radius profile of a Tapered Optical Fiber [29]

These tapered fibers differ from usual optical fibers because of the vanishing of the original silica core [31]. At the waist, the silica clad acts like a core, while the surrounding medium acts like a clad, leading to a strong refractive index difference. This contrast modifies the intensity distributions and the polarization orientations of the field and its components [31]. However, tapered fibers have known particular properties like high power density at the fiber surface and cylindrical asymmetry in the field distribution [32], large penetration length of the evanescent wave [33], enhancement of the power fraction of the field outside the fiber [33, 34], and large waveguide dispersion [34].

4.2.2 Implementation

The production of the cavity fiber was done in two steps: first, the implementation of the two Bragg grating mirrors, and second the pulling of the fiber.

Bragg grating A fiber Bragg grating is a Bragg reflector constructed in the core of an optical fiber. It consists of a periodic variation of the refractive index, creating a dielectric mirror for one specific wavelenght. In this case, the goal is to obtain a cavity for the D_2 transition of the ^{87}Rb: it needs two gratings for a wavelenght of 780 nm.

The two gratings do not have exactly the same properties: one has a 1% transmission, whereas the other one has a 9% transmission. This

allows us first to distinghish the two outputs, but also to select one or the other according to the current measurements, reducing or increasing the signal before the photon detectors.

In order to have an operable cavity, the gratings properties must be exactly right: they were installed in ten optical fibers, but after testing, only three were good enough to be kept.

Pulling of the fiber The next step is to pull the fiber to a nanometer waist scale inorder to be able to get strong radial confinement of the light, allowing efficient and controlled interactions with matter [30, 31, 35, 36]. The way to obtain such fibers is by using a flame pulling method (more details in [35]). The transformation of the fiber modes needs to be adiabatic, so that the transmission remains high, and that the light efficiently couples in and out of the fiber.

This step is also quite tidious, as the fibers easily break if the pulling is not done correctly. Out of the three cavity fibers already selected, only one survived the pulling: this is why only one cavity fiber was put inside the chamber.

Surroundings Once placed in the chamber, the outputs of the fiber were spliced to two fibers X, as shown in figure 4.4. It is 99-1% X-fibers: the input power is splitted into the two outputs, 99% of the power in one and only 1% in the other.

Figure 4.4: Cavity surroundings

This way, it is possible to measure at the same time in transmission and in reflection, and to choose the considered mirror of the cavity. It is also possible to send in two different lights and to look at only one in output, even if the X-fiber splitting is not perfect, as we will see in the chapter about the optical force.

4.2.3 Control

In order to control the mode frequencies of the cavity, only the cavity length can be changed. It is done with the piezo plates to which the fiber is glued. The piezo voltage is controlled by a Labview programm, which lock the cavity to the right frequency. To do so, one needs a reference light with a strong enough signal.

Most of the time, the reference light is the cooler light. Even if the cooler laser is not guided into the fiber, a lot of its light still coupled into the nanofiber, and its signal is powerful enough to lock the cavity on it. An other option is to use a light running directly through the fiber, for example the imaging light, constantly on in this case.

The main inconvenient in using the cooler light is the great noise of the signal. It could be explain by some interferences between the beams, coming from the same source and thus coherent, resulting in a plane wave below the chip (see figure 4.5), visible because of the fiber vibrations.

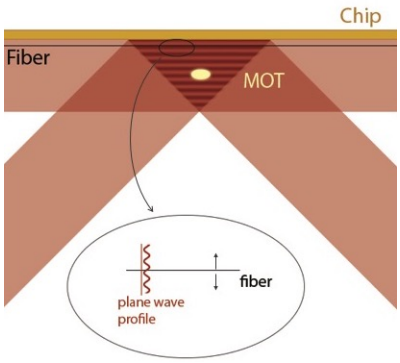

Figure 4.5: Position of a plane wave below the chip, due to interference between the beams. As the fiber is constantly vibrating, it could explain the huge noise in the cooler signal

This noise is not present when the lock uses the imaging light guided by the fiber. The signal is then very smooth and the lock really stable. However, the cooler light can not be turned off: as soon as the two frequencies are sufficiently close, both signals are amplified by the cavity and a lock is therefore impossible. That is why a lock with the fiber imaging, however smooth the signal may be, is in reality not as stable as it looks.

The cavity is locked with the cooler light ; however, during the measurement times, all lights are turned off for around 50 ms. It is not a

problem for the cavity which can stay stable for around 100 ms. It is even possible to detune the cavity only for the measurement time, making a jump in the piezo voltage, while it is locked with the cooler whose frequency stays the same.

4.2.4 Utilisation

By locking the cavity with the cooler light, one needs to be careful about the birefringes of the cavity. The cavity is indeed a birefringent medium, which means that the refractive index slightly depends on the polarization of the light.

Now, the cooler light is not linearly polarize: the two components of the polarization have therefore slightly different resonance frequencies, which leads to two different peaks when swipping the piezo voltage.

However, for the measurement, the imaging light needs to be in resonance with the cavity, and is linearly polarize. That is why it is necessary to align the imaging polarity axis with one axis of the cavity, and to lock the cavity to the cooler resonance of this same polarization axis.

In practice, it is quite easy to check before running measurements. Once the cavity is locked on one of the cooler resonances, one needs to let the imaging sweep around the resonance, unlocked.

By looking at the single shot counts, one will see some peaks: they correspond to the component of the linearly polarized imaging light along the axis on which the cavity is locked. They need to be maximise, i.e. the polarization axis of the imaging needs to be align to the chosen one of the cavity. It is simply done with a $\lambda/2$ plate before the coupling into the fiber.

If no peaks are visible, it means that the imaging light is already more or less aligned with the other axis, and by locking the cavity to the next cooler resonance, one should see some.

4.3 Rupture of the cavity

As explained above, when the cavity was fabricated, only one fiber passed all the steps. There were thus no choice to make, and it was put in the chamber in 2014, and treated with good care as some properties were not tested (for example how much power to send in without breaking it). Usually, ultrathin nanofibers such as this one are preselected according to their resistance, and still have a lifetime of around one year and a half.

After more than two years, our cavity deteriorated and broke, preventing us to finish some measurements

4.3.1 Finesse

The cavity being hard to lock from some time already, at some point, the birefringes of the cavity became very hard to see, which is very uncommon. The cavity resonance seemed much broader and the birefringes peaks were always there, but as single peaks, no matter the orientation of the $\lambda/2$ plate

So to have a better look, instead of making a sweep of the imaging with the cavity locked, a piezo sweep was made with only the cooler light turned on. This way, it gives the course of the transmission curve as a function of the cavity length, and the pairs of peaks corresponding to both polarization axis should be presents.

Two parameters of the cavity can be easily deduced from this kind of curve:

- the FSR or Free-Spectral Range, i.e. the frequency distance between two consecutive resonances. It is done by rescaling the time axis (or piezo-voltage axis, as the sweep is supposed to be linear) to a frequency axis : by using two lasers whose the frequency detuning is known

- the finesse of the cavity, as the ratio of the distance between two consecutive resonances and the half width of one resonance

As these parameters were already measured before, if they happen to be far from their previous values, this could be a first indicator of any important change in the cavity properties.

The first strange observation, while having only the cooler light, was that only single broad peaks were visible (see figure 4.6a). By turning the $\lambda/2$ plate, and therefore the polarization axis of the light, only the intensity of the signal changed, but the peaks stayed of the same height, no ratio involved. Which allowed us to refute the idea that each peak corresponded to one polarization, with a FSR which would have been much larger than before.

This was moreover confirmed by the real measurement of the FSR, around 1300 MHz, same as before.

This lead us to the first conclusion that the two polarization resonances simply overlaped, causing this broad peak. Which was more or less confirmed by the strict measurement of the finesse, around 5.7, i.e. more than ten times smaller than before.

After this conclusion, the experiment was turned off, including the Rb dispenser. But after a couple of days off, and still with the dispenser off, the exact same measurement was made again, and this lead to normal results (figure 4.6b), with a much better finesse and the bifringes visible again.

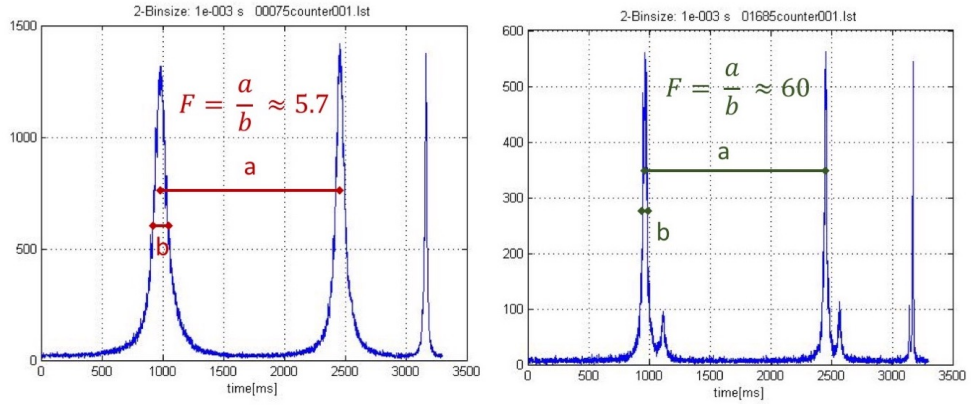

(a) Transmission with the dispenser on: low finesse, unusual results

(b) Transmission with the dispenser off: high finesse, usual results

Figure 4.6: Piezo sweeps before the rupture of the cavity. The piezo voltage is increasing during 3000 ms before decreasing again.

However, by turning on the dispenser again and after a couple of hours, the problem was back: a solution needed to be found.

4.3.2 Sticking atoms

Obviously, this strange behaviour is due to the Rubidium atoms in the chamber. After some investigations, we learned that when using this kind of ultrathin fibers, and expecially when loading a MOT on or very close to the fiber, which was exactly the case at this point, a lot of atoms stick to the fiber surface and can alter the fiber properties. The solution to this is usually to send in continuously some high power light to avoid the atoms to stick. Which is one of the main reasons why the usual

nanofibers are first selected by testing their resistance to high power (up to 20 mW), while in our case, we always sent in a coupled of hundreds microwatts at most.

The particularity of our fiber is that we had no idea how much power it could support, as it was never tested for fear of breaking our only cavity. We also would have needed a laser of different frequency to not interfere with the cavity lock, and to be easily filtered on output. And most of the time, the MOT was load away from the fiber, and only then guided with a short ramp to the fiber. So a lot of atoms were lost during the ramp, and only a small number of them actually reached the fiber, at the point were the MOT was turned off, so they did not stay long at the surface: we never really had to realise such process.

4.3.3 Dust

In order to solve the cavity finesse problem, some high power (up to 3 mW) was send into the fiber to remove the atoms from the surface, with the dispenser just turned off: the finesse stayed very low. So around 2 mW were then continuously send in for a couple of days: the birefringes did not show up again, the behaviour was still exactly the same.

By looking more precisely at the fiber with a side camera, we could see a point of unusual loss: this was certainly due to some dust (or a bunch of atoms) sticking to the fiber. A loss of this type reduces a lot the transmission of an optical fiber, and in this case, a lower transmission means a much worst cavity, and explained the low finesse. It is also really risky to remove it: the only way we could achieve it was by sending some light in, and hope that the heat would make it go away. But in the vacuum chamber, no convection are possible: the only heat transfers are radiative. If the dust is not removed quick enough, it will radiate at the fiber surface and could damage it. But there was no other choice.

So the power of the laser sent in was increased, while looking at the fiber to turn it off as soon as the dust was removed. Such an operation had already been made with the usual fiber, and was succesful in about half a minute. However, it was not the case for the cavity fiber: the dust heated up and broke the fiber, which now has a zero transmission.

5 Detection

Both absorption and fluorescence are common detection methods. They use a resonant probe light in order to get the photons absorbed by the atoms, and spontaneously re-emitted in random directions. Some properties can also be easily measured by the imaging system in single shots pictures. All methods have different strengths which will be presented here.

5.1 Absorption

The absorption of resonant probe light by atoms in the detection region is often used to detect atoms and estimate atom densities in magnetic or magneto-optical traps [15, 37].

5.1.1 Theory

The **absorption** method (see figure 5.1) consists in sending in some known resonant probe light whose photons will be absorbed by the atoms. They will be spontaneously re-emitted but in a random direction.

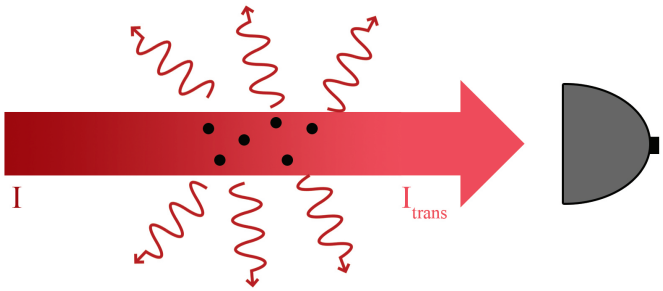

Figure 5.1: Absorption principle. The detector measures the remaining probe light after passing through the atoms

The detector measures what is left of the probe light. Under the condition of an illumination below saturation ($\delta = 0, I < I_{sat}$), the **Beer-Lambert's law** can be applied:

$$I_{tr} = Ie^{-\rho_{at}\sigma_0} \qquad \rho_{at} = \frac{n_{at}}{A}$$

where σ_0 is the scattering cross section, I the incident intensity, I_{tr} the transmitted intensity and ρ_{at} the column density of n_{at} atoms over the area A.

The scattering cross section is obtain under the two-level system approximation. Indeed, the only possible transition on the D_2 line is the $5^2S_{1/2}, |F = 2, m_F = \pm 2\rangle \longrightarrow 5^2P_{3/2}, |F = 3, m_F = \pm 3\rangle$: the smallest spacing between adjacent hyperfine states is larger than 72 MHz, for a probe light linewidth of $\Delta\nu$ <1 MHz.

So in the limit of weak pumping light, the scattering cross section is given by:

$$\sigma_0 = \frac{\hbar\omega_0\Gamma}{2I_{sat}}$$

$$\omega_0 = \frac{E_2 - E_1}{\hbar} \qquad \Gamma = \frac{1}{\tau} \approx 2\pi \cdot 6MHz$$

with E_1 and E_2 the ground and excited state, so ω_0 is thus the transition frequency, and Γ is the natural linewidth (FWHM) of the transition with a lifetime $\tau = 26.24$ ns.

Back to the Beer-Lambert's law, the maximum cross section for the ^{87}Rb D_2 line is $\omega_0 = 0.29\ \mu m^2$ [38]. So one atom per μm leads to a maximal absorption of around 25%. Thus, for a cylindrical interaction region of cross section $A = 20\ \mu m^2$, we approximately have 1.5% absorption per atom.

5.1.2 Experimental implementation

In absorption detection, the imaging is coupled into the considered fiber. With the usual fiber, the only measurement possible is in transmission, whereas with the cavity, it can be done in transmission or in reflection (see figure 5.2).

After the MOT being loaded and guided to the fiber, all lights are turned down except for the imaging. The atoms are in the area of the evanescent field and can therefore absorb some photons. The transmitted intensity is then lower than the incident one, whereas the refected one is higher.

With the cavity, the atoms signal stays longer: more than 10 ms, while with the usual fiber the atoms are only visible for 3 ms.

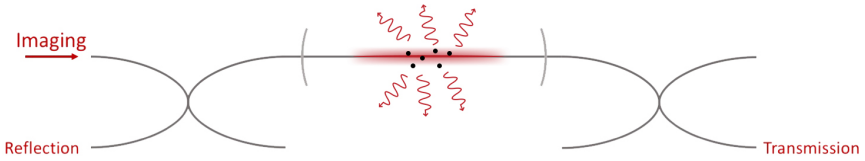

Figure 5.2: Implementation of absorption detection with the cavity fiber. The atoms are in the region of the evanescent field, and absorb some photons from the coupled imaging light.

5.1.3 Advantages and drawbacks

First, absorption is a destructive method: it alters the atoms state and expells them from the interaction region. However, no non-destructive methods could be used in this set-up for practical reasons.

Signal-to-noise ratio Assuming that the incoming light intensity I is known and constant, the signal-to-noise ratio only depends on the transmitted intensity measurement I_{tr}, which can not be more precise than the shot noise limit.

The incoming intensity I is given by:

$$I = \frac{E}{TA} = \frac{n_{ph}hc}{T\lambda_f A}$$

with E the energy and T the measurement time.

The signal-to-noise ratio in absorption is then given by:

$$SNR_{abs} = \frac{IT - I_{tr}T}{\sqrt{I_{tr}T}} = \frac{IT(1 - e^{-\rho_{at}\sigma_0})}{\sqrt{ITe^{-\rho_{at}\sigma_0}}}$$

$$SNR_{abs} = \sqrt{IT}\ \frac{1 - e^{-\rho_{at}\sigma_0}}{\sqrt{e^{-\rho_{at}\sigma_0}}}$$

If we are only concerned about single atoms detection, the assumption that $\rho_{at}\sigma_0 \ll 1$ can be made. This way, the SNR can be simplified to:

$$\boxed{SNR_{abs} \approx \sqrt{IT}\rho_{at}\sigma_0 = n_{at}\frac{\sigma_0}{A}\sqrt{IT}}$$

In this case, the absorption signal-to-noise ratio is proportionnal to the atom number in the detection region.

So with $SNR_{abs} = 1$, the smallest detectable atom number is:

$$\boxed{n_{at,min}^{abs} \approx \frac{A}{\sigma_0\sqrt{IT}}}$$

Subsequently, different options could lead to an increase in the absortion detector sensitivity:

- a decrease of the detection region A. Unfortunately, not only the spot size is a critical limit for the coupling to the atom [39, 40]), but in our setup, the light is fiber guided and it is therefore impossible to change the focus

- an increase of the interaction time T. This also leads to a scattering of the atoms, which would heat up and leave the interaction region, but can be very efficient in addition to dipole traps [41, 42] or for ions [43, 44].

Finally, one also needs to know the atom number uncertainty Δn_{at}. It is defined as the ratio of the shot noise and the number of photons scattered per atoms m, which gives in absorption:

$$\boxed{\Delta n_{at}^{abs} = \frac{photon - shot - noise}{signal - per - atom} = \frac{\sqrt{IT}}{m}}$$

What is noticeable here is that the atom number uncertainty is independent from the actual atom number. However, it depends on the shot noise, which is usually not small enough to detect single atoms. Only in the strong coupling regime can the signal per atom be increased, and therefore is absorption detection very efficient.

Theoretically, there is no limit in absorption detection efficiency, and it could detect single atoms [45]. However, the smaller the atom number is, the smaller the difference between incident and transmitted energy is (around 1.5 % per atom), and the absorption signal become easily hidden by fluctuations ; especially since the full intensities have to be measured, hence highly sensitive detector can not be used.

Nevertheless, it is very efficient for counting large number of atoms in optically dense ensembles.

5.1.4 Typical measurements

In this experiment, absorption detection is used when a strong signal is needed, or when one needs to compare signals : typically for detuning scans in order to find the resonance, or in B-field scans to find the best configuration to guide the atoms to.

In figure 5.3 are shown some examples of absorption measurements. Both are a mean of several shots of the same configuration: atoms may be visible in single shots in absorption, but the signal is naturally way smoother after a mean of several shots.

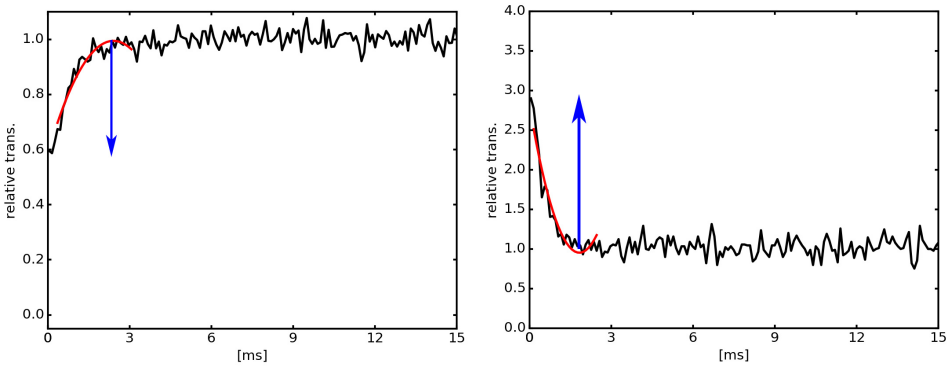

(a) usual fiber, in transmission (b) cavity fiber, in reflection

Figure 5.3: Absorption measurements with both fibers, means of several shots. The signal is defined as the high of the dip, represented by the blue arrows.

Both measurements were realised with some flashes, after a ramp: the MOT was loaded away from the fiber, in order to be bigger and denser. After the loading time, it was guided through the considered fiber using a ramp in the magnetic field of around 300 ms. Once at the fiber, cooler and repumper are turned off and the imaging is turned on for a flash of around 50 ms. The turning off of the other lasers is not absolutely necessary but allow to reduce noise, which is always better ; and to have less signal to measure, which is important for the photon detector. Indeed, our SPCMs are linear only up to 1000 counts per ms, and saturate and could be damage with signal higher than 15000 counts per ms.

However, as the MOT lasers are off, the atoms quickly leave the detection area: they are only visible for a couple of miliseconds. The intensity

of the absorption signal is then given by the high of the peak left by the atoms in the first miliseconds.

In figure 5.3a, the measurement is realised with the usual fiber, so in transmission: the received signal is lower with atoms than without. It is naturally inverted in reflection, as we can see in figure 5.3b, realised with the cavity fiber.

As those measurements are quite efficient, and only need a few single shots to have a nice result, it is very convenient to use for large scans, typically a B-field scan, an example of which is given in figure 5.4

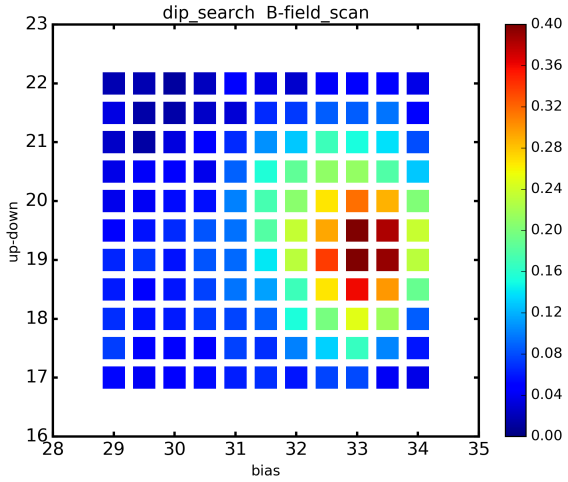

Figure 5.4: Magnetic field scan in absorption, using the cavity in transmission: the signal intensity corresponds to the depth of the dip.

5.2 Fluorescence

The fluorescence method is an other common method of atomic detection, more efficient in the case of single emitters [14].

5.2.1 Theory

The **fluorescence** method also consists in exciting the atoms using a resonant probe light, but to measure this time the photons reemitted by them (see figure 5.5). The lifetime of the excited state ($\tau = 26.24$ ns for

the ^{87}Rb D_2 line) being very short, all absorbed photons are immediately reemitted in the whole 4π solid angle.

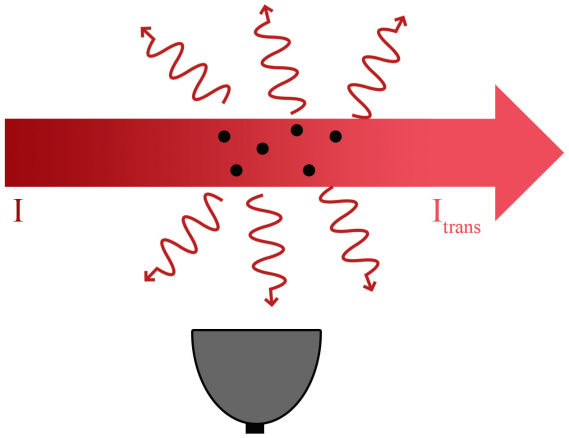

Figure 5.5: Fluorescence principle

No detector can collect all of those photons: only a fraction η_{coll} is measured, leading to an estimation of the total number of scattered photons n_{ph}^{scatt}.

The Beer-Lambert's law is still valid: the scattered intensity is given by:

$$I_{scatt} = I - I_{tr} = I \cdot (1 - e^{-\rho_{at}\sigma_0})$$

And the measured intensity, assuming that the detector is linear:

$$I_{fluo} = \eta_{coll} \cdot I_{scatt} = \eta_{coll} \cdot I \cdot (1 - e^{-\rho_{at}\sigma_0})$$

5.2.2 Experimental implementation

In our experiment, the detector is the fiber: therefore, the detection region must be around the fiber surface, in order to couple some scattered photons into the fiber.

To do so, the imaging laser is send into the chamber towards the fiber, orthogonaly (see figure 5.6). The light is only send as flashes at the time when the atoms reach the fiber. This way, they are excited close to the fiber and a consequent part of them can coupled into it. However,

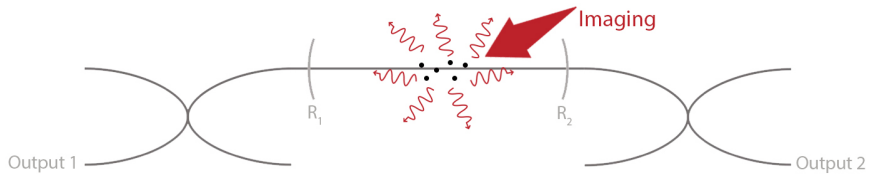

Figure 5.6: Implementation of the fluorescence detection. The imaging beam excites the atoms at the surface of the cavity, where some scattered photons can coupled into the fiber

the beam being orthogonally directed, the non-scattered photons do not coupled in and are not detected by the SPCMs.

The signal can be measured with both outputs, the only difference being the transmission of the corresponding mirror.

5.2.3 Advantages and drawbacks

As for absorption, the main disadvantage of fluorescence detection is that it is a destructive method. However, as previously said, the setup complexity of non-destructive methods forbids them to be used in our experiment.

Signal-to-noise ratio In fluorescence measurement, the signal corresponds to the intensity of the scattered photons coupled into the fiber I_{fluo}. Under the assumption of no other background sources during the measurement, the background light only comes from the fraction f_{bg} of the incoming photons scattered by anything else but the atoms, which coupled into the fiber:

$$I_{bg} = I \cdot \eta_{coll} \cdot f_{bg}$$

Which gives for the signal to noise ratio:

$$SNR_{fluo} = \frac{I_{fluo}T}{\sqrt{(I_{fluo} + I_{bg})T}} = \sqrt{T\eta_{coll}I}\frac{1 - e^{-\rho_{at}\sigma_0}}{\sqrt{1 - e^{-\rho_{at}\sigma_0} + f_{bg}}}$$

So in the case of a small atom number, and thus $\rho_{at}\sigma_0 \ll 1$, it simplifies as:

$$\boxed{SNR_{fluo} \approx \sqrt{T\eta_{coll}I}\frac{\rho_{at}\sigma_0}{\sqrt{\rho_{at}\sigma_0 + f_{bg}}}}$$

And on top of that, if we assume a background free measurement ($f_{bg} = 0$), the optimal signal-to-noise ratio in fluorescence is:

$$SNR_{fluo}^{opt} = \sqrt{T\eta_{coll} I \rho_{at} \sigma_0} = \sqrt{\frac{T\eta_{coll} I \sigma_0}{A}} \cdot \sqrt{n_{at}}$$

One notes that in fluorescence, $SNR_{fluo} \propto \sqrt{n_{at}}$.

Concerning the minimum detectable atom number, we again obtain it for a SNR equal to 1:

$$\boxed{n_{at,min}^{fluo} = \frac{A}{T\eta_{coll} I \sigma_0}}$$

And finally, the atom number uncertainty is once again the ratio between the photon shot nois and the signal per atom:

$$\Delta n_{at}^{fluo} = \frac{photon - shot - noise}{signal - per - atom} = \frac{\sqrt{\eta_{coll} n_{at} m}}{\eta_{coll} m}$$

$$\boxed{\Delta n_{at}^{fluo} = \sqrt{\frac{n_{at}}{\eta_{coll} m}}}$$

So we also have $\Delta n_{at}^{fluo} \propto \sqrt{n_{at}}$, which means that fluorescence is a very effective method to detect a few atoms.

As for absorption, there is theoretically no limit to the detection efficiency, if the interaction time T can be increased, and if of course the background is low enough.

A big advantage of the fluorescence method is that the probe light is not collected by the detector, but only a portion of the scattered light. That means that the measured intensity is quite small and therefore, very sensitive photons detectors can be used. So with a sufficiently low background, fluorescence is actually more efficient in detecting single atoms than absorption, even considering the limited collection efficiency [14].

5.2.4 Typical measurements

The challenge in fluorescence measurement is the alignement of the imaging beam with the atoms. Indeed, the imaging beam is quite focused: around 5 mm diameter. Sometimes it even goes through a focussing lens first in order to focused the beam even more and have higher power on the atoms. And it needs to be directed exactly at the place were the atoms meet the fiber. It is all the more tidious as there is no way to know this place precisely, neither to know exactly were the beam is. The only way is to try to find the right place using the different cameras and looking at beam reflexions, and runing some scans to improve the position. It is even longer as the atoms are not visible in single shot but need at least a mean of a couple of shots.

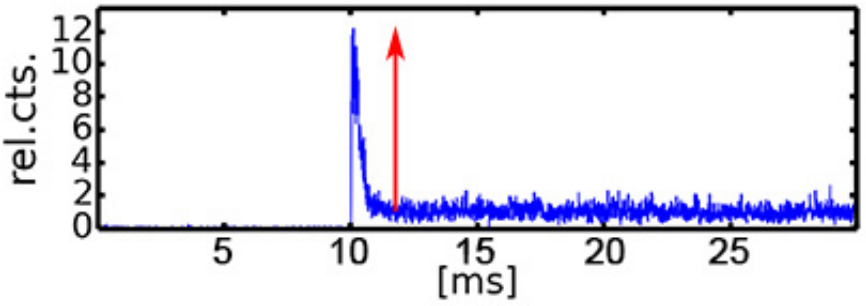

Figure 5.7: Fluorescence measurement in relative counts. The high of the peak is proportionnal to the atom number, represented by the red arrow.

An example of a fluorescence measurement is given in figure 5.7: the SPCMs are turned on after 10 ms, at the moment where the MOT reached the fiber: the atoms are visible for around 3 ms, after which the signal decrease quickly to reach the background floor.

6 Photon antibunching

Light beams can be classified according to their photon statistics. While some of them have classical explaination, others are typical proof of the quantum nature of light. This is the case for the antibunched light emitted by single atoms.

6.1 Second order correlation function

The second order correlation function quantifies the way the intensity fluctuates over time:

$$g^{(2)}(\tau) = \frac{\langle I(t)I(t+\tau)\rangle}{\langle I(t)\rangle\langle I(t+\tau)\rangle}$$

with $I(t)$ the intensity of the light beam at the time t and $\langle..\rangle$ a time average. Considering a spatially coherent light from a small area of the source, the second order correlation function actually represents the temporal coherence of light.

In a classical approach, the time scale of the intensity fluctuations is ruled by the coherence time τ_c of the source [8]: if $\tau \gg \tau_c$, the fluctuations between t and $t+\tau$ will be uncorrelated, and therefore $\langle I(t)I(t+\tau)\rangle_{\tau\gg\tau_c} = \langle I(t)\rangle^2$, which leads to :

$$g^2(\tau \gg \tau_c) = 1$$

So the g^2 function tends to 1 for high values of τ.

Conversely, for $\tau = 0$, there is some correlations: for any time dependance of $I(t)$,

$$g^{(2)}(0) = \frac{\langle I(t)^2\rangle}{\langle I(t)\rangle^2} \geqslant 1$$

and even, for any classical light:

$$g^{(2)}(0) \geqslant g^{(2)}(\tau)$$

6.2 Bunched, antibunched and coherent light

Consequently, this second order correlation function can be used to classified different types of light, using the initial value of the $g^{(2)}$ function:

- bunched light: $g^{(2)}(0) > 1$, compatible with classical results,
- coherent light: $g^{(2)}(0) = 1$, compatible with classical results,
- antibunched light: $g^{(2)}(0) < 1$, no classical explanation

Each of them also corresponds to different photon streams.

Bunched light Bunched light corresponds to light with $g^{(2)}(0) > 1$, and as the name suggests, the photons come together as bunches (see figure 6.1). The statistical distribution is super-Poissonian.

Figure 6.1: Bunched light photon streams. Photons regroup as bunches, which is a manifestation of their bosonic nature [8]

If photons come as bunches, that means that once a photon is detected, the probability to detect a new one is higher right after it than after a longer time. So $g^{(2)}(\tau)$ is higher for small τ, which is consistent with the classical predictions : $g^{(2)}(0) > g^{(2)}(\infty)$.

In a classical interpretation, photon bunching is linked to the intensity fluctuations of a chaotic light (see figure 6.2). The bunches correspond indeed to the high intensity levels, as the photon number is proportionnal to the instantaneous intensity. Conversely, the time intervalls during which the intensity is lower than the average correspond to lacks of bunches.

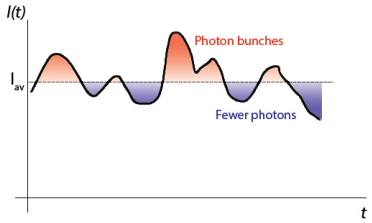

Figure 6.2: Link between chaotic light fluctuations and photon bunching in a chaotic source

Coherent light A perfectly coherent light has $g^{(2)}(0) = g^{(2)}(\tau) = 1$ for all values of τ. The photon streams of such light is therefore absolutely random (see figure 6.3), the photon statistic is Poissonian [8]. It is possible to observe two photons at the same time.

Figure 6.3: Coherent light photon streams: the time intervals between photons are random

The probability of detecting a photon is the same for all time intervals: this is a manifestation of the randomness of the Poissonian photon statistic.

Antibunched light An antibunched light corresponds to photons streams with a minimum time interval between them (see figure 6.4).

Figure 6.4: Antibunched light photon streams

That means that the probability of detecting a photon right after another one is low, whereas it is higher for longer τ. We therefore obtain:

$$g^{(2)}(0) < g^{(2)}(\tau)$$
$$g^{(2)}(0) < 1$$

This is obviously not compatible with classical results: antibunching of light is purely quantum.

The second order correlation function of an antibunched light has two possible profiles (see figure 6.5).

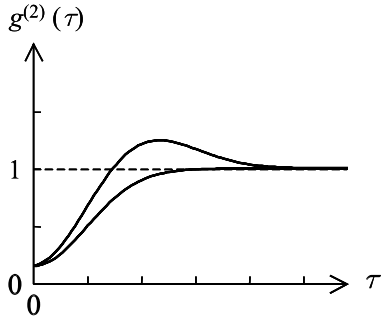

Figure 6.5: $g^{(2)}$ profiles for an antibunched light: $g^{(2)}(0) < 1$ [8]

Even if they often appear together, it is important to notice that photon antibunching and sub-poissonian photon statistics are not the same phenomena [46]. They are both manifestations of the quantum nature of light, but are not directly connected. It is even possible to observe sub-Poissonian statistics with bunched light.

6.3 Detection

In order to detect the antibunching of light, one needs to isolate the emitted species and regulate the emission rate, as it was first discovered in [47]. In our case, it means to detect single atoms of Rubidium.

The sequence is illustrated in figure 6.6: if an atom absorbs a photon at $t = 0$, it stays in an excited state for around τ_R, i.e. the radiative lifetime, before reemiting the photon. Once the photon is reemitted, the atom will absorb a new photon shortly afterwards, if the laser power is high enough. Which will once again be re-emitted after a time $\sim \tau_R$, and the emission cycle will start again.

The spontaneous emission of photon is a probabilistic process: the emission time is not stricly constant, and fluctuates around τ_R. However, the probability to have an emission time $\ll \tau_R$ is very small, which means $g^{(2)}(0) \approx 0$.

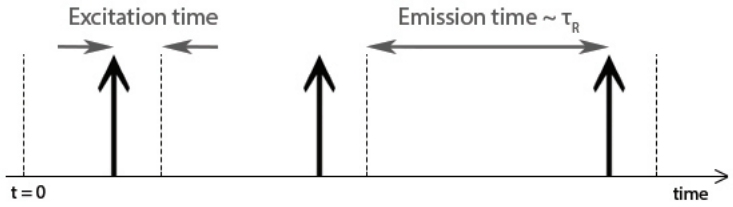

Figure 6.6: Photon emission cycle: the dashed lines correspond to the absorption of a photon by the atoms, the arrows to their re-emission

The important point in the detection of this phenomenon is to observe light emitted from a single atom. If the light is emitted by several atoms, the emission cycle is no longer observable, as they are all independent, and it is impossible to distinguished which photon is emitted by which atoms.

Experimental implementation The antibunching of light is obviously detectable only with very few atoms: the first difficulty in the experimental implementation is to make single atoms couple into the fiber. The MOT is therefore loaded closer to the fiber than before, but still slightly away from it. This way, only a peripheral atom would be close enough to couple into it.

The idea was to use fluorescence: it is indeed the most effective method to detect single atoms (see [14]). However, the measurements are usually used in flashes: after the loading of the MOT, all lasers are turned off except for a flash of the imaging, whose light will be scattered by the atoms and coupled into the fiber. This type of measurement gives a very short signal of a couple of milliseconds. Yet, in order to observe the antibunching of light, one needs a lot of statistics, and with only 30 milliseconds of signal for each 10 seconds cycle, one would need to run the scan for a very long time to be able to see something. This is why the first try was to constantly measure the fluorescence of the signal, using the cooler light to excite the atoms, with every lasers on, and to remove the floor afterwards.

In order to remove the floor, a part of the measurement must be without atoms. To do so, they are removed using a magnetic field ramp,

which leads the MOT towards the chip where it will be crushed. The first cycle was made of three subcycles, and the crossing of the MOT through the fiber was clearly visible (see figure 6.7)

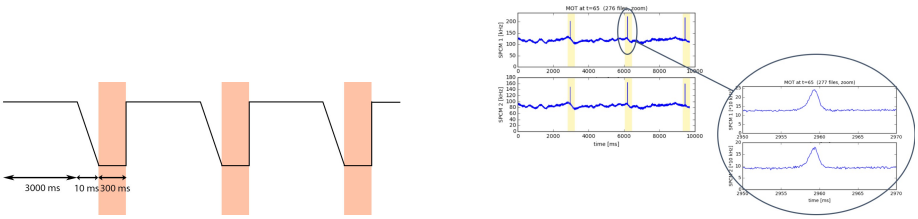

(a) Magnetic field cycle with three subcycles. Highlighted, the moment without atoms

(b) Mean intensity of one cycle with three subcycles (Highlighted, the moment without atoms), and zoom on the part where the atoms cross the fiber, before being crushed on the chip.

Figure 6.7: Cycle with three subcycles

It is visible in figure 6.7b that the 300 ms without atoms are too short to reach the floor: the photons stay indeed in the cavity for a longer time. The cycle was then changed to only one ramp after 6 seconds with atoms (see figure 6.8): the ramp lasted 300 ms, followed by around 3 second without any MOT. We see that the signal needs this couple of seconds before reaching the floor.

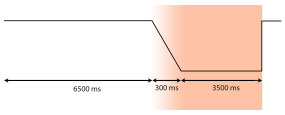

(a) cycle with only one ramp

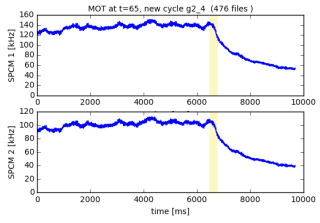

(b) one ramp: mean intensity. Highlighted: the magnetic ramp

Figure 6.8: cycle with one ramp

In our setup, the use of two detectors is very useful: the goal is to correlate all the counts, in order to plot the time interval between them.

One detector could theoretically be enough, but an autocorrelation of the counts could lead to a distortion of the $g^{(2)}$ function due to afterpulse [14]. This is avoided by using two detectors and making cross-corelations: the signal is then distorted because of secondary emissions, but this is easilly corrected.

With the cavity fiber, different outputs are available: the first idea was to measure the signal from two different ones, corresponding to the two different gratings of the cavity. However, the difference of transmission of the mirrors (1% and 9%) was disturbing to correlate the signals. Besides, all the lasers (and expecially the cooler) being constantly on, the intensity was too high for the SPCMs and it needed to be filtered. Only one output was therefore used, from which the signal was filtered and divided (see figure 6.9)

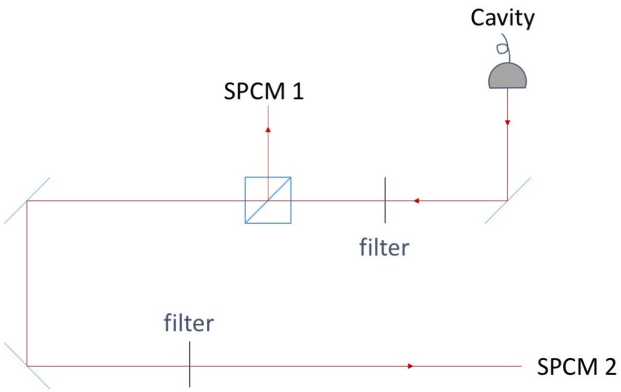

Figure 6.9: Implementation of the detectors

From this setup, the two signals can be correlate after the floor being removed, and could be enough to observe the antibunching of light

Data processing The main difficulty of the data processing is to take into account all the noise in the signal. A first measured normalised correlation function was defined in 1978 [48] as:

$$\overline{g_S^{(2)}}(\tau) = \frac{\overline{G^{(2)}}(\tau)}{|\overline{G^{(1)}(0)}|^2}$$

with $\overline{G^{(2)}}(\tau)$ the average over the Poisson distribution of the second-order correlation function. But if the observation region A is larger than a coherence area A_C, the function needs modification to take into acount the spatial averaging of the signal :

$$\overline{g_S^{(2)}}(\tau) = 1 + \frac{1}{(1+\delta/\bar{N})^2}(|g_A^{(1)}(\tau)|^2 f(A) + \frac{2\delta}{\bar{N}} Re(g_A^{(1)}(\tau)) f_D(A) + \frac{g_A^{(2)}(\tau)}{\bar{N}})$$

with:

- $\bar{N}$ the atom number within the scattering volume, averaged over the Poisson distribution,
- ϵ a time-independent term describing the scattered light from the background,
- $\frac{1}{\delta} = \frac{I_A}{|\epsilon|^2}$ is the signal to noise ratio for a single atom
- $f(A)$ and $f_D(A)$ are complicated functions given explicitly in [49], which are equal to 1 for $A \ll A_C$ and go to zero as $1/A$ for $A \gg A_C$

The antibunching effect is actually only contained in the third term inside the brackets. The two first terms are indeed heterodyne terms (beating of light from different atoms, and fluorescent light with the background light, respectively). Those two first terms, absent and present simultaneously, represent the background noise and mask the antibunching effect: it can only be measure with $A \gg A_C$, and for a very small number of scaterers. A very low background is therefore essential.

In order to simplify the data processing, the previous function being complicated to use, a simpler relation as been given in [50], where all the background light is compiled:

$$g^{(2)}(\tau) = \frac{C_N(\tau) - (1-\rho^2)}{\rho^2}$$

with $C_N(\tau) = \dfrac{c(\tau)}{N_1 N_2 \omega T}$, where:

- $c(\tau)$ is the raw coincidence,
- N_1 and N_2 are the single count rates of each detector,
- ω is the time bin,

- T is the integration time

and $\rho = \dfrac{S}{S+B}$, with S the signal light and B the background light, which is measured independently in each experimental run.

The last formula is the one used in the data processing.

6.4 Background issues

The data were aquired and processed. Unfortunately, the background noise was still too high: the wanted signal is indeed very low, as it only comes from single atoms. The removing of the background needs to be very efficient to obtain a nice result, which was not the case in our measurement (see figure 6.10)

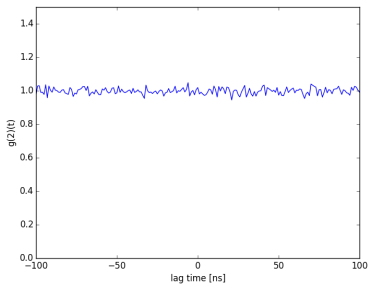

Figure 6.10: Try to plot the $g^{(2)}$ function, with an integration time of 5 seconds. No dip is visible, most probably because of the high background

Several attempts were made to try to reduce the background, which should not be that high considering that no light is directly coupled into the fiber. The cooler light, in particular, is responsible for the main part of the background, even if it should not couple into the fiber. The light probably coupled into it at some particular points, for example around the taper or by refraction in the glue spots (see figure 6.11). But those parts of the beams are actually useless, as they only need to superimpose at the MOT location. So by shadowing the outer part of the diagonal beams (by reducing the aperture) and the upper part of the horizontal ones (using a sheet of paper), the number of cooler photons coupling into the fiber should decrease a lot.

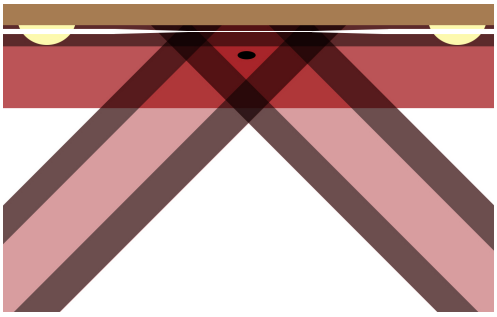

Figure 6.11: Shadowing attempt of the light beams

Before shadowing the beams, the mean intensity with the cavity on resonance was around 60 kHz. After shadowing them, it only lowers up to 50 kHZ: this is unfortunately not enough to hope for a better $g^{(2)}$, and the setup was changed.

The background of this setup is very high because the detectors are constantly acquiring: the acquisition last during the whole cycle, with all the lasers on. The best solution would be to measure only with the imaging on, which would lower the background a lot. However, it would need to alternate long time intervals of loading the MOT, and short pulses of measurement time. So to get enough data, i.e. the same total measurement time as before, one would need much longer scans.

However, the need to reduce the background is inevitable. The next scan was also planned in fluorescence, but this time using the imaging light to excite the atoms, and with 10 subcycles in every cycle: the flashes would be shorter as before so that the MOT does not have the time to evaporate completely, and so that it does not need a long loading time afterward (see figure 6.12).

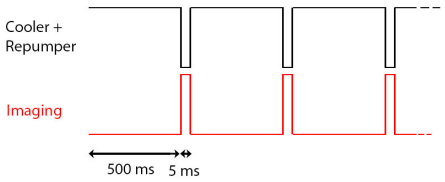

Figure 6.12: New cycle scheme in absorption

To do so, the adwin program was not quick enough, and some external frequency generators were used, triggered by the adwin, and turning on

and off the lasers as well as the SPCMs to measure only during the flashes.

Unfortunately, the cavity broke during the implementation of this setup: no scan were made and the antibunching of light was not observed for our experiment.

7 Optical dipole force

After the rupture of the cavity, some measurements were still possible only with the usual fiber: the optical dipole force on the atoms, using some high power blue detuned light. Generating a new shape of potential, with a barrier next to the fiber, should repelled the atoms from sticking to the fiber and therefore lead to a longer signal.

7.1 Atom-light interaction

Theory When light goes through a medium, the dipole moments of the atoms align with the electric field vector of the light. Knowing the electric susceptibility of the medium, $\chi(\omega)$, dependent on the frequency, the total polarization $\vec{P}$ can be written as:

$$\vec{P} = \epsilon_0 \chi(\omega) \vec{E}$$

This leeds [14] to a reduction of the speed of light in the medium by a factor $\frac{1}{\sqrt{1+\chi}}$ with respect to c, and a refractive index $n = \sqrt{1+\chi}$, which can also be written as:

$$n(\omega) = n_r + i \cdot \frac{\alpha}{2 \cdot \frac{\omega}{c}}$$

Two phenomena can be noticed in this formula: the dispersion, represented by the real part $n_r = Re(n)$, and the absorption, represented by the imaginary part, with $\alpha = \frac{2\omega}{c} Im(n)$.

In the Lorentz-model of the interaction of light and matter [14], the dispersion relation is given by:

$$n(\omega) = 1 + \frac{n_e q_e^2}{2\epsilon_0 m_e((\omega_0^2 - \omega^2) - i\rho\omega)}$$

with q_e and m_e the charge and mass of the electron, n_e the electronic density, ω_0 the resonance frequency and ρ the damping factor of the electrons oscillations.

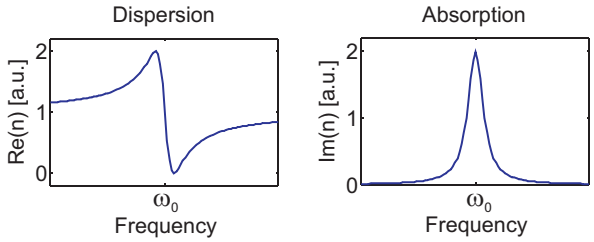

Figure 7.1: Real (dispersion) and imaginary (absorption) part of the complex refractive index [14]

This two phenomena have different influences on the system: the two profiles are plotted in figure 7.1. Concerning the dispersion, the slope changes sign close to the resonance, where the dispersion is anomalous. Far away from it, the dispersion is normal and proportional to $1/\omega$. The absorption, however, is proportional to $1/\omega^2$: it thus is dominant only close to the resonance.

Application This property is useful to build a barrier of potential, using the dispersion. In our case, the goal is to counterbalance the Van der Waals potential, which leads the atoms to stick to the fiber surface. To do so, a new light is send in the fiber, blue-detuned in order to repel the atoms. The detuning must be big enough for the absorption to be negligible; however, if the detuning is too big, one would need a bigger power to detect the effects of the dispersion force. And as explained in section 4, we would like to avoid sending too much power in the fiber at the risk of burning it. Thus, a compromise must be found, taking of course into account the available laser wavelenght: the chosen blue light had a wavelenght of 767 nm, i.e. a detuning $\Delta\omega = 2\pi \cdot 6.538$ THz.

The introduction of a new light field aroung the fiber leads to a new potential (see figure 7.2). Without blue light, only the Van der Waals potential is present, leading the atoms towards the fiber. By adding a sufficiently powerful blue light, a new potential adds up, depending on the light intensity [31].

7.2 Dipole force

The presence of this barrier of potential can lead to different effects on the atoms:

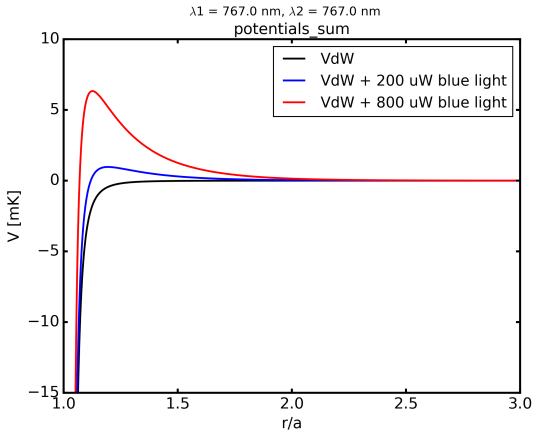

Figure 7.2: Potentials simulation close to the fiber surface, as a function of the ratio r/a, with r the distance from the fiber center and a the fiber radius. In black, without any blue light; in blue, with a $200\mu W$ blue light; in red with a $800\mu W$ blue light

- the MOT is further away from the fiber: the signal should be **weaker** than before
- the barrier prevents the atoms from sticking to the fiber surface: the signal should be **longer**
- the atoms are further away: the resonance peak should be **less symmetrical** with higher power [30]
- the new electrical field should lead to a Stark effect [51]: the resonance should **shift** towards the blue frequencies.

Indeed, if the atoms are away from the fiber, only the photons from the outer part of the MOT, less dense, can coupled into the fiber, and the signal is thus reduced.

The presence of the barrier of potential should delay the atoms from sticking to the fiber surface.

Very next to the fiber, the MOT does not behave the same according to the detuning of the probe light [30], and two phenomena add up (see figure 7.3):

- The trajectory of the atoms close to the fiber are different, as the blue light repels them while the red one attracts them (figure 7.3 b and c)

- On the other hand, due to the attraction, the interaction time for the red light is much shorter, as the velocity and therefore the atomic loss rate are higher

Those two effects actually compensate each other very close to the fiber (closer as 100 nm), but further away, the red detuned light leads to a lower density than the blue one [30].

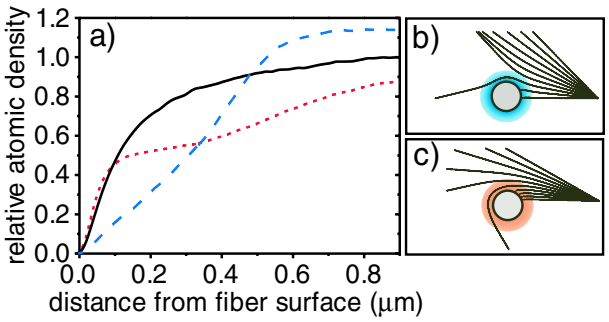

Figure 7.3: Simulations of the relative density of the MOT for different detunings δ of the imaging light [30]: in solid black $\delta = 0$ MHz, in dotted red $\delta = -3$ MHz, in dashed blue $\delta = +3$ MHz. b) and c) show several atomic trajectories for $\delta = +3$ MHz (b) and $\delta = -3$ MHz (c)

This affects the shape of the resonance dip, when scanning the imaging detuning. Indeed on the first part, when the detuning is negative, i.e. red, the density tends to be lower, and leads to a weaker signal, while it is the opposite for the blue detuning. This asymetry becomes stronger the further the atoms are from the fiber:

- This effect is negligible close to the fiber [30], where the atoms are without any blue light (see figure 7.2). The scan is therefore supposed to be quite symetrical

- With a blue light around $200\mu W$, the atoms stay at a distance r with $r/a \approx 1.5$; i.e. with $a = 0.2\mu m$, $r \approx 0.3\mu m$, the distance for which the density difference starts (figure 7.3)

- For a blue light around $800\mu W$, $r/a \approx 2.0$, which leads this time the atoms to a distance $r \approx 0.4\mu m$: the effect is non negligible and the scan should be clearly asymetrical

Finally, the presence of a new electrical field leads to a Stark effect [51]. The far detuned light of the blue laser acts like a perturbation in the second order of the electric field, i.e. linear in terms of field intensity. The interaction Hamiltonian is therefore $H_{int} = -\widehat{\mu}\mathbf{E}$, with $\widehat{\mu} = -e\mathbf{r}$ representing the electric dipole operator. For a two-level atom like in our case, this reduces to $H_{int} = -\mu\mathbf{E}$ and the energy shift between the ground and the excited state is given by [51]:

$$\Delta E = \pm\frac{|\langle e|\mu|g\rangle|^2}{\delta}|E|^2 = \pm\frac{3\pi c^2}{2\omega_0^3}\frac{\Gamma}{\delta}I$$

with Γ the decay rate and δ the detuning.

In the case of a blue detuning, the two states come closer to each other (see figure 7.4), unlike a red light which can be used as a potential trap.

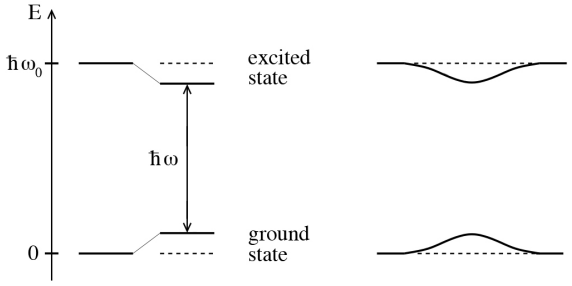

Figure 7.4: Energy shift induced by the Stark effect of a far blue detuned light

7.3 Implementation

The setup for this measurement needs again to minimize the background. Indeed, both imaging light and blue detuned light must be coupled in the fiber, but only the imaging must be measured. The blue light is too powerful (from 200 μW to 1 mW) to be sent on the sensitive SPCMs.

The first idea was to use an X-fiber on one side of the nanofiber, like in figure 7.5. Unfortunately, this did not work because the background from

the blue light was too high, even with two good filters before the SPCMs: it seemed like some of the blue light scattered back in the X-fiber and came back at around 780 nm on the other output.

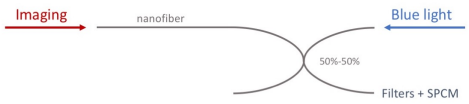

Figure 7.5: First setup idea using a fiber-X

Instead, a polarized beam splitter was used, which was much more efficient (figure 7.6), still with both lights counterpropagating in the nano fiber.

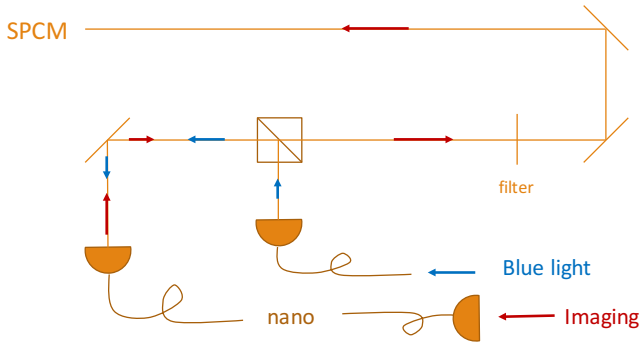

Figure 7.6: Experimental set-up for the optical dipole force measurement

The scans were realised in absorption, with 4 subcycles per cycle (see figure 7.7). The MOT is loaded away from the fiber and guided towards it for the measurement, during which the cooler and repumper lasers flash off.

The blue light is constantly on, and therefore adds some inevitable background that needs to be removed. That is why for a measurement time of 30 ms in total, the imaging is on for only 15 ms: it is more than enough to see the atoms signal, and the mean of the last 15 ms corresponds to the floor to remove from the previous 15 ms, which limits the intensity fluctuations uncertainties.

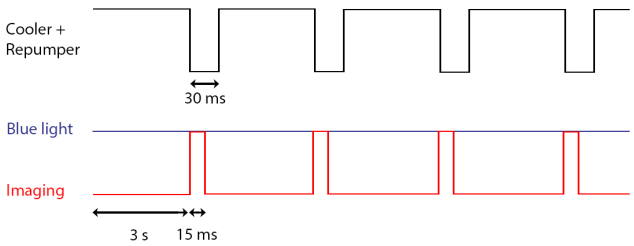

Figure 7.7: Cycle for the optical dipole force measurement

7.4 Results and discussion

6 scans were realised with different powers of blue light: no blue light at all, 200 μW, 400 μW, 600 μW, 800 μW and 1 mW. They are all ploted together in figure 7.8, and separated in two plots for a better visibility in figure 7.9.

The four previous expectations can now be discussed.

Intensity of the signal Concerning the intensity of the signal, the measurement corresponds to what was expected: the more powerful the blue light is, the less intense the signal. This can be the direct consequence of a MOT further away, due to the potential barrier.

Symmetry of the signal The scans were fitted by an asymmetrical lorentzian [52]: in the usual symmetrical lorentzian formula

$$L(\nu) = \frac{2A/\pi\gamma_0}{1 + 4[(\nu - \nu_0)/\gamma_0]^2}$$

the γ_0 coefficient was replaced by:

$$\gamma(\nu) = \frac{2\gamma_0}{1 + exp(a(\nu - \nu_0))}$$

which introduce the a parameter as a measure of asymmetry, $a = 0$ corresponding to a symmetrical curve.

This a parameter is the one written in the legends of figures 7.8 and 7.9. As expected, the asymmetry tends to become more important with higher power of the blue light, in conjunction with an eventual atomic position further away from the fiber.

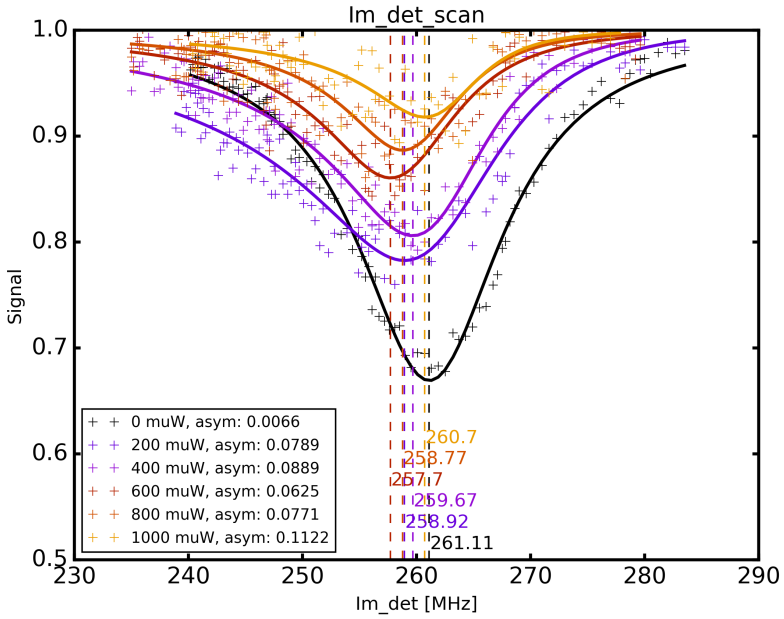

Figure 7.8: All results: the depth of the signal as a function of the imaging laser's detuning. Each color corresponds to a different power of the blue laser. The parameter on the legend box represents the asymmetry of the fit, 0 corresponding to a symmetrical one. The colored coordinates are the minima of each plot.

Frequency shift Concerning a shift of the frequency resonnance, none is obviously visible. Aside from the last scan at 1 mW blue light, which signal is very low and therefore quite uncertain, the frequency resonance seems to slightly shift towards smaller frequencies, but they all stay very close to one another and it could only be experimental fluctuations.

In order to have a better idea of the expected shift, a numerical calculation was made. From [51], the energy shift ΔE is given by:

$$\Delta E = \hbar\Delta\omega = \pm\frac{3\pi c^2}{2\omega_0^3}\frac{\Gamma}{\delta}I$$

The detuning δ in the formula corresponds to the detuning of the blue light with the atomic transition:
Atomic transition: $\omega_0 = 2\pi \cdot 384.227$ THz [38]
Blue light: $\omega_1 = 2\pi\dfrac{c}{\lambda} = 2\pi \cdot 391.032$ THz
Detuning: $\delta = \omega_1 - \omega_0 = 2\pi \cdot 6.538$ THz

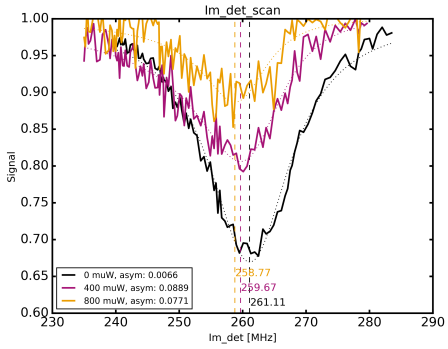

(a) 0, 400 and 800 μW

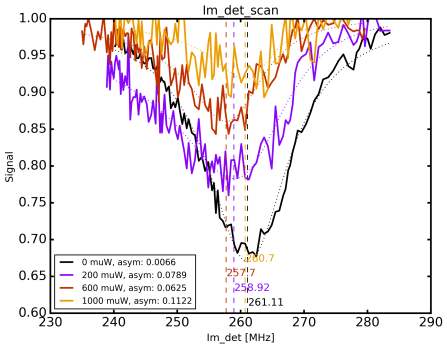

(b) 0, 200, 600 and 1000 μW

Figure 7.9: Separated scans: each color corresponds to one different power of the blue laser, the legend parameter indicates the asymmetry and the colored coordinate the minimum of each plot.

The decay rate of the ^{87}Rb D_2 line is $\Gamma = 2\pi \cdot 6.065$ MHz [38].

The intensity of the light next to the fiber can be calculated from [31]: the simulated intensities for different powers of blue light are plotted in figure 7.10.

Thus, very next to the fiber, the field intensity is of the order of 10^9 W/m^2 (figure 7.10a). However, it decays quite quickly, and at the most probable location of the atoms, it is more in the order of 10^7 W/m^2 (figure 7.10b).

So numerically this gives us:

$$\hbar\Delta\omega \approx \frac{3\pi \cdot (2.997 \cdot 10^8)^2}{2(2\pi \cdot 384.227 \cdot 10^{12})^3} \frac{2\pi \cdot 6.065 \cdot 10^6}{2\pi \cdot 6.538 \cdot 10^{12}} 10^7$$

$$\hbar\Delta\omega \approx 2.791 \cdot 10^{-28} \text{ J.Hz}$$

Which means
$\Delta\omega \approx 2.646$ MHz

This number corresponds to the experimental results: the shift is not bigger than a couple of MHz. Unfortunately, this is also the order of magnitude of the experimental error: even if a tendency seems to mani-

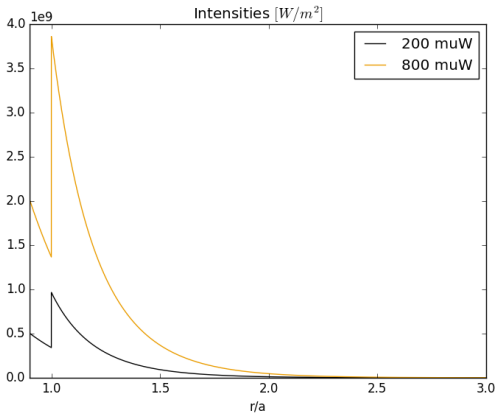

(a) Global view

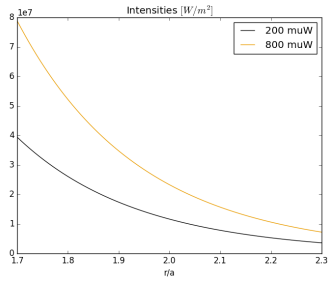

(b) zoom around the MOT location

Figure 7.10: Intensity simulations next to the fiber for a blue light of 200 μW and 800 μW, depending on the distance r from the fiber center, with a the radius of the fiber

fest itself, it is hard to assure that it is a physical phenomenon and not experimental fluctuations.

Duration of the signal The last assumption to check is the duration of the signal. To see if the presence of the blue barrier actually prevents the atoms from sticking to the fiber, one needs to compare the duration of each signal. To do so, mean intensity in resonance for each blue power were normalized and streched so that the signal goes down to zero for a better lisibility. Plotted together, the slops of the signal are easily comparable (see figure 7.11).

What comes out of those graphs is that the blue light presence and power has no impact on the duration of the signal. The atoms seem to be present for the same time around the fiber, no matter of the blue barrier of potential. However, it is important to notice that the atoms are quite warm (a few hundreds μK): the measurement being done when the MOT is off, the cloud expand very quickly, leading to a low density hard to detect with the usual fiber. So the fact that the signal is not longer does not necessarily mean that the blue barrier does not work.

So actually, from the four assumptions made previously:

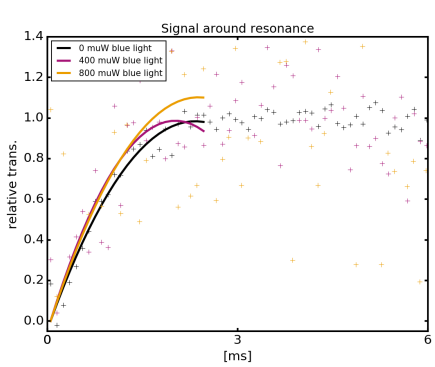

(a) Blue light at 0, 400 and 800 μW

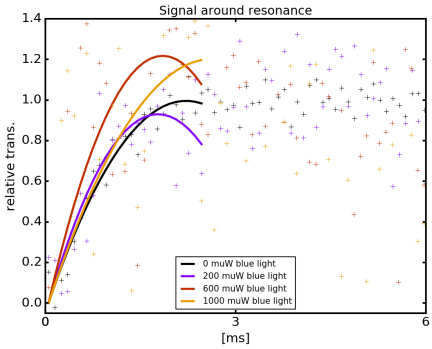

(b) Blue light at 0, 200, 600 and 1000 μW

Figure 7.11: Normalized signals around the resonnance

- The intensity of the signal is smaller as the blue light power increases, as expected.
- The signal is less symmetric as the blue light power increases, as expected.
- A shift tendency may be visible, even though it is in the order of experimental fluctuations. However, it corresponds to the numerical simulation.
- The signal duration is the same no matter the blue light power, unlike what was expected.

7.5 Atoms and fiber surface interactions

The continuous use of blue light led to some other unexpected observations. During the realisation of the different scans, the blue light was at some point turned off in order to realise again the scan without it. As expected, very quickly (around 30 seconds), the transmission of the fiber went down, as the atoms of Rubidium began to stick to the surface, as explained in section 4. However, the atomic signal was still visible and the scan was started.

After some hours, however, the transmission started to rise again. The scan was therefore extended in order to observe this rise until the end. In figure 7.12 are plotted the main intensity of each file. The two lower

steps at the end correspond to a time when the imaging laser was out of lock

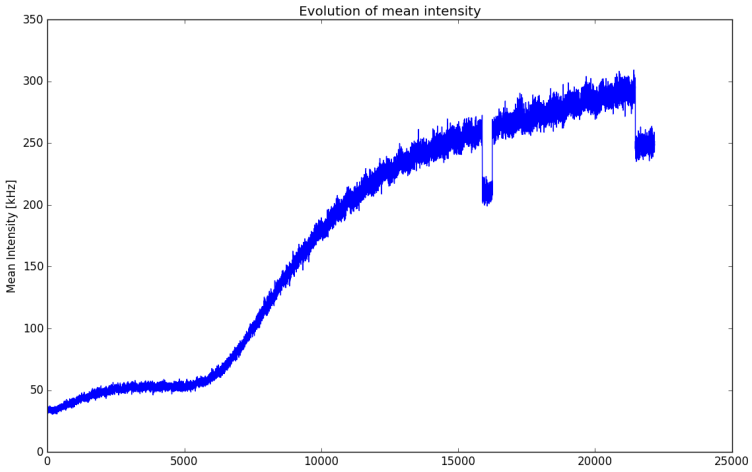

Figure 7.12: Mean intensity evolution, just after turning off the blue light. The x axis corresponds to file numbers but in time, it goes up to around 30 hours. The two steps at the end correspond to the imaging getting out of lock.

This phenomena, which was already observed, is rather unexpected. If the atoms stick to the fiber in the absence of any light inside it, they do not have any reason to leave after a couple of hours. And no other parameter should intervene with time: there is no obvious explanation and this point still needs to be studied.

8 Conclusion and outlook

This work has presented several measurements of atomic detection, realised with a nanofiber cavity and an atomchip. This new association leads to a hybrid quantum system with a good detection efficiency, thanks to some particular properties:

- The independance between the atomic trap and the fiber cavity is quite unusual in Cavity Quantum Electrodynamics. The trapping is indeed carried out by the Magneto Optical Trap and has no relation with the cavity control: the center of mass motion is completely decoupled from the light within the cavity.
- The light-matter interactions are intense and very well controled in the region of evanescent light field, around the fiber waist. This enables very precise measurements.

The single atom detection, attempted with the measurement of the photon-photon autocorrelation function $g^{(2)}$, was not succesful, since the cavity broke before the end of the measurements. However, there are sufficient reasons to believe that this would have been achievable, since the Signal to Noise Ratio was expected to be better, and since similar measurements were already made in a previous set-up. The possibility of a single atom detector with this kind of system is therefore not excluded.

The interactions between the atoms and the fiber surface have for their part been well studied in this thesis. The constant use of a blue detuned light in the fiber would improve the system: not only will it prevent the atoms to stick to the surface, reducing the losses, ie increasing the transmission and thus the finesse ; but it could also eventually increase the lifetime of a colder atom cloud.

Outlook A first improvement to make could be about the cavity. This implementation used one pair of Bragg gratings: if the control was not bad using the light from the cooler laser, it could be improve by the use of a second pair of Bragg gratings, setted for an other wavelenght. This

way, the control would be done with a far detuned laser coupled into the fiber, allowing a smooth signal and a fine control, as well as an easy filtering.

An other possibility for the cavity would be the implementation of a ring cavity. By splicing both ends of a nanofiber to an X-fiber, with a 99/1 % ratio, one can easily build a cavity. Its properties would be defined according to the transmission of the fiber, and could lead to high finesse.

The next step of development would be a better use of the quasi one dimensionality of the components: the fiber geometry would perfectly fit a one-dimensional trap, easily achievable with the atom chip. In particular, the implementation of a Bose-Einstein Condensate coupled to a nanofiber would certainly present numerous advantages to existing set-ups and lead to new informations on condensate.

Bibliography

[1] P. A. M. Dirac, *The Principles of quantum mechanics.* oxford uni ed., 1930.

[2] N. Bohr, "The Quantum Postulate and the Recent Development of Atomic Theory," *Nature*, vol. 121, pp. 580–590, 1928.

[3] C. N. Cohen-Tannoudji, "Manipulating atoms with photons," *Review of Modern Physics*, vol. 70, no. 3, p. 707, 1998.

[4] H. J. Metcalf and P. van der Straten, *Laser Cooling and Trapping.* springer ed., 1999.

[5] M. H. Anderson, J. R. Ensher, M. R. Matthews, C. E. Wieman, and E. A. Cornell, "Observation of Bose-Einstein Condensation in a Dilute Atomic Vapor," *Science*, vol. 269, p. 198, 1995.

[6] S. N. Bose, "Plancks Gesetz und Lichtquantenhypothese," *Z. Phys*, vol. 26, p. 178, 1924.

[7] R. Folman, P. Krüger, J. Schmiedmayer, J. Denschlag, and C. Henkel, "Microscopic atom optics: from wires to an atom chip," *Advances in Atomic, Molecular, and Optical Physics*, vol. 48, pp. 263–356, 2002.

[8] M. Fox, *Quantum Optics, An introduction.* Oxford University Press, 2006.

[9] P. D. Lett, W. D. Phillips, S. L. Rolston, C. E. Tanner, R. N. Watts, and C. I. Westbrook, "Optical molasses," *Journal of the Optical Society of America B*, vol. 6, no. 11, p. 2084, 1989.

[10] D. J. Wineland and W. M. Itano, "Laser cooling of atoms," *Physical Review A*, vol. 20, no. 4, pp. 1521–1940, 1979.

[11] M. Weidemüller and C. Zimmermann, *Cold Atoms and Molecules.* Wiley, 2009.

[12] E. S. Shuman, J. F. Barry, and D. Demille, "Laser cooling of a diatomic molecule," *Nature*, vol. 467, pp. 820–823, 2010.

[13] M. Wilzbach, *Single atom detection on an atom chip with integrated optics*. PhD thesis, 2007.

[14] D. Heine, *Single Atom Detection and Non-Classical Photon Correlations*. PhD thesis, TU Wien, Universität Heidelberg, 2008.

[15] W. Ketterle, D. S. Durfee, and D. M. Stamper-Kurn, "Making, probing and understanding Bose-Einstein condensates," *Proceedings of the International School of Physics "Enrico Fermi"*, p. 67, 1999.

[16] S. Chu, "The manipulation of neutral particles," *Review of Modern Physics*, vol. 70, no. 3, pp. 685–706, 1998.

[17] W. D. Phillips, "Laser cooling and trapping of neutral atoms," *Review of Modern Physics*, vol. 70, no. 3, p. 721, 1998.

[18] D. E. Pritchard, "Cooling Neutral Atoms in a Magnetic Trap for Precision Spectroscopy," *Physical Review Letters*, vol. 51, no. 15, p. 1336, 1983.

[19] W. Petrich, M. H. Anderson, J. R. Ensher, and E. A. Cornell, "Stable, Tightly Confining Magnetic Trap for Evaporative Cooling of Neutral Atoms Wolfgang," *Physical Review Letters*, vol. 74, no. 17, pp. 252–255, 1995.

[20] C. E. Wieman and L. Hollberg, "Using diode lasers for atomic physics," *Review of Scientific Instruments*, vol. 62, no. 1, pp. 1–20, 1991.

[21] L. Ricci, M. Weidemüller, T. Esslinger, A. Hemmerich, C. Zimmermann, V. Vuletic, W. König, and T. W. Hänsch, "A compact grating-stabilized diode laser system for atomic physics," *Optics Communications*, vol. 117, no. 5-6, pp. 541–549, 1995.

[22] M. G. Littman and H. J. Metcalf, "Spectrally narrow pulsed dye laser without beam expander.," *Applied optics*, vol. 17, no. 14, pp. 2224–2227, 1978.

[23] R. Folman, P. Krüger, D. Cassettari, B. Hessmo, T. Maier, and J. Schmiedmayer, "Controlling Cold Atoms using Nanofabricated Surfaces: Atom Chips," *Physical Review Letters*, vol. 84, no. 20, pp. 4749–4752, 2000.

[24] J. Reichel, W. Hänsel, and T. W. Hänsch, "Atomic Micromanipulation with Magnetic Surface Traps," *Physical Review Letters*, vol. 83, no. 17, pp. 3398–3401, 1999.

[25] M. Wilzbach, *Aufbau eines Experiments zur miniaturisierten und integrierten Detektion neutraler Atome*. PhD thesis, 2002.

[26] E. A. Donley, T. P. Heavner, F. Levi, M. O. Tataw, and S. R. Jefferts, "Double-pass acousto-optic modulator system," *Review of Scientific Instruments*, vol. 76, no. 063112, 2005.

[27] "LL01-780 Datasheet," 2007.

[28] M. Wagner, *Bachelorarbeit : Zusammenbauen und Testen eines Imagingsystems für Atomchip Experimente Inhaltsverzeichnis*. PhD thesis, 2014.

[29] A. Stiebeiner, R. Garcia-Fernandez, and A. Rauschenbeutel, "Design and optimization of broadband tapered optical fibers with a nanofiber waist.," *Optics express*, vol. 18, no. 22, pp. 22677–85, 2010.

[30] G. Sagué, E. Vetsch, W. Alt, D. Meschede, and A. Rauschenbeutel, "Cold-atom physics using ultrathin optical fibers: Light-induced dipole forces and surface interactions," *Physical Review Letters*, vol. 99, no. 16, pp. 1–4, 2007.

[31] F. Le Kien, J. Q. Liang, K. Hakuta, and V. I. Balykin, "Field intensity distributions and polarization orientations in a vacuum-clad subwavelength-diameter optical fiber," *Optics Communications*, vol. 242, pp. 445–455, 2004.

[32] J. Bures and R. Ghosh, "Power density of the evanescent field in the vicinity of a tapered fiber," *Journal of the Optical Society of America A*, vol. 16, p. 1992, aug 1999.

[33] V. I. Balykin, K. Hakuta, F. Le Kien, J. Q. Liang, and M. Morinaga, "Atom trapping and guiding with a subwavelength-diameter optical fiber," *Physical Review A*, vol. 70, no. 011401, 2004.

[34] L. Tong, J. Lou, and E. Mazur, "Single-mode guiding properties of subwavelength-diameter silica and silicon wire waveguides," *Optics Express*, vol. 12, no. 6, p. 1025, 2004.

[35] G. Sagué, A. Baade, and A. Rauschenbeutel, "Blue-detuned evanescent field surface traps for neutral atoms based on mode interference in ultrathin optical fibres," *New Journal of Physics*, vol. 10, no. 113008, 2008.

[36] F. Le Kien, V. I. Balykin, and K. Hakuta, "Atom trap and waveguide using a two-color evanescent light field around a subwavelength-diameter optical fiber," *Physical Review A*, vol. 70, no. 063403, 2004.

[37] M. Wilzbach, A. Haase, M. Schwarz, D. Heine, K. Wicker, X. Liu, K. H. Brenner, S. Groth, T. Fernholz, B. Hessmo, and J. Schmiedmayer, "Detecting neutral atoms on an atom chip," *Fortschritte der Physik*, vol. 54, no. 8-10, pp. 746–764, 2006.

[38] D. A. Steck, "Rubidium 87 D Line Data," *Journal of Geophysical Research*, vol. 2009, no. 2, p. 31, 2010.

[39] S. J. Van Enk and H. J. Kimble, "Strongly focused light beams interacting with single atoms in free space," *Physical Review A*, vol. 63, no. 023809, 2001.

[40] S. J. Van Enk, "Atoms, dipole waves, and strongly focused light beams," *Physical Review A*, vol. 69, no. 043813, 2004.

[41] D. Frese, B. Ueberholz, S. Kuhr, W. Alt, D. Schrader, V. Gomer, and D. Meschede, "Single Atoms in an Optical Dipole Trap: Towards a Deterministic Source of Cold Atoms," *Physical Review Letters*, vol. 85, no. 18, pp. 3777–80, 2000.

[42] R. Grimm and M. a. P. H. I. a. S. Weidemuller, "Optical Dipole Traps," *Advances in Atomic, Molecular and Optical Physics*, vol. 42, pp. 95–170, 2000.

[43] D. Leibfried, R. Blatt, C. Monroe, and D. Wineland, "Quantum dynamics of single trapped ions," *Review of Modern Physics*, vol. 75, no. 1, pp. 281–324, 2003.

[44] C. E. Wieman, D. E. Pritchard, and D. J. Wineland, "Atom cooling, trapping, and quantum manipulation," *Review of Modern Physics*, vol. 71, no. 2, pp. S253–S262, 1999.

[45] D. J. Wineland, W. M. Itano, and J. C. Bergquist, "Absorption spectroscopy at the limit: detection of a single atom," *Optics Letters*, vol. 12, no. 389, 1987.

[46] X. T. Zou and L. Mandel, "Photon-antibunching and sub-Poissonian photon statistics," *Physical Review A*, vol. 41, no. 1, pp. 475–476, 1990.

[47] H. J. Kimble, M. Dagenais, and L. Mandel, "Photon antibunching in resonance fluorescence," *Physical Review Letters*, vol. 39, no. 11, pp. 691–695, 1977.

[48] H. J. Carmichael, P. Drummond, P. Meystre, and D. F. Walls, "Intensity correlations in resonance fluorescence with atomic number fluctuations," *Journal of Physics A: Mathematical and General*, vol. 11, no. 5, pp. L121–L126, 2001.

[49] E. Jakeman, "Photon correlation," in *Photon correlation and light beating spectroscopy*, springer ed., 1974.

[50] R. Brouri, A. Beveratos, J.-P. Poizat, and P. Grangier, "Photon antibunching in the fluorescence of individual color centers in diamond," *Optics Letters*, vol. 25, no. 17, p. 1294, 2000.

[51] R. Grimm, M. Weidemüller, and Y. Ovchinnikov, "Optical dipole trap for neutral atoms," *Adv. At. Mol. Opt. Phys.*, vol. 42, p. 95, 2000.

[52] A. L. Stancik and E. B. Brauns, "A simple asymmetric lineshape for fitting infrared absorption spectra," *Vibrational Spectroscopy*, vol. 47, no. 1, pp. 66–69, 2008.